Archives of Civil and Mechanical Engineering (2025) 25:24
https://doi.org/10.1007/s43452-024-01067-5

ORIGINAL ARTICLE

Active learning on stacked machine learning techniques for predicting compressive strength of alkali-activated ultra-high-performance concrete

Farzin Kazemi[1,2] · Torkan Shafighfard[3] · Robert Jankowski[1] · Doo-Yeol Yoo[4]

Received: 9 April 2024 / Revised: 27 July 2024 / Accepted: 28 September 2024

Abstract
Conventional ultra-high performance concrete (UHPC) has excellent development potential. However, a significant quantity of CO_2 is produced throughout the cement-making process, which is in contrary to the current worldwide trend of lowering emissions and conserving energy, thus restricting the further advancement of UHPC. Considering climate change and sustainability concerns, cementless, eco-friendly, alkali-activated UHPC (AA-UHPC) materials have recently received considerable attention. Following the emergence of advanced prediction techniques aimed at reducing experimental tools and labor costs, this study provides a comparative study of different methods based on machine learning (ML) algorithms to propose an active learning-based ML model (AL-Stacked ML) for predicting the compressive strength of AA-UHPC. A data-rich framework containing 284 experimental datasets and 18 input parameters was collected. A comprehensive evaluation of the significance of input features that may affect compressive strength of AA-UHPC was performed. Results confirm that AL-Stacked ML-3 with accuracy of 98.9% can be used for different general experimental specimens, which have been tested in this research. Active learning can improve the accuracy up to 4.1% and further enhance the Stacked ML models. In addition, graphical user interface (GUI) was introduced and validated by experimental tests to facilitate comparable prospective studies and predictions.

Keywords Machine learning algorithm · Alkali-activated ultra-high performance concrete · Active learning algorithm · Compressive strength · Hyperparameter optimization

✉ Farzin Kazemi
farzin.kazemi@pg.edu.pl

✉ Doo-Yeol Yoo
dyyoo@yonsei.ac.kr

Torkan Shafighfard
tshafighfard@imp.gda.pl

Robert Jankowski
jankowr@pg.edu.pl

[1] Faculty of Civil and Environmental Engineering, Gdańsk University of Technology, Ul. Narutowicza 11/12, 80-233 Gdańsk, Poland

[2] Department of Structures for Engineering and Architecture, School of Polytechnic and Basic Sciences, University of Naples "Federico II", Naples, Italy

[3] Institute of Fluid Flow Machinery, Polish Academy of Sciences, Generała Józefa Fiszera 14, 80-231 Gdańsk, Poland

[4] Department of Architecture and Architectural Engineering, Yonsei University, 50 Yonsei-Ro, Seodaemun-Gu, Seoul 03722, Republic of Korea

1 Introduction

For improving building and infrastructure operation and safety and satisfy sustainability standards, various engineering sectors must adopt environmentally friendly practices through technological innovations and scientific breakthroughs. Ultra-high-performance concrete (UHPC) was developed in the mid-1990s to meet these needs [1]. UHPC is a composite material based on ordinary Portland cement (OPC) that combines high-volume fractions of high-strength microsteel fibers with highly cementitious ingredients with a low water-to-binder (W/B) ratio. These materials provide advantages such as high durability, exceptional toughness, and extremely high compressive strength (> 150 MPa). Over the past 20 years, they have been used in the construction industry, including hydraulic and offshore structures and overlay materials. Bridges, restoration and retraining, and windmill towers are other useful applications of UHPC [2, 3]. However, overusing ordinary Portland cement can result

Published online: 12 November 2024

in significant carbon dioxide emissions, as the OPC within UHPC is approximately 5–7 times greater than that of conventional concrete [4].

Recently, the development of enhanced concrete based on an alkali-activated method has been proposed for its sustainable and functional goals. The benefits of cementless alkali-activated UHPC (referred to as "AA-UHPC" hereafter) include a lower carbon footprint, lower heat of hydration while curing, waste reduction, and outstanding durability [5, 6]. The mechanical properties of AA-UHPC are similar to those of UHPC, but AA-UHPC outperforms UHPC in terms of sustainability. One of the most important properties of UHPC structures is compressive strength because these materials are subjected to compressive loads in different applications. Abdellatief et al. [7] investigated geopolymer UHPC using fine ceramic waste with replacements up to 22.5%. Their findings suggest that ceramic waste can be optimized for eco-friendly geopolymer UHPC with enhanced high-temperature resistance and minimal negative effects on mechanical properties and durability. According to Provis and Van Deventer [8], geopolymer binders emit carbon dioxide, which is approximately 50–80% less than that emitted by OPC binders. The binder material used in AA-UHPC does not include cement, as it uses fly ash (FA) and ground-granulated blast furnace slag (GGBS), which are inorganic materials rich in Si and Al, combined with alkaline activators to create binders [9]. However, some researchers have highlighted the importance of using AA-UHPC as an alternative to traditional cement-based UHPC for structures subjected to extreme loadings [10].

Extensive experimental studies have been conducted to understand the effects of various factors on the compressive strength of AA-UHPC. An experimental study was conducted to investigate the compressive strengths of FA- and GGBS-based alkali-activated concrete with different mix proportions [11]. Results showed that controlling factors such as GGBS/binder, W/B, and curing time had a more significant effect on the compressive strength of these materials than water content. In addition, the mechanical prediction model accurately captured the experimental case study. Different densities of GGBS-, and FA-based alkali-activated concrete were developed based on mechanical test results [12]. Alkali-activated concrete has greater compressive strength than regular concrete made of Portland cement with the same density. The benefits of adding reinforcing fibers were also highlighted, as the compressive strength of alkali-activated concrete with a 0.5% fiber volume fraction was significantly improved. The effects of the addition of steel fibers on the mechanical attributes of AA-UHPC were thoroughly investigated [13]. The addition of steel fibers did not necessarily increase the compressive strength of these materials, although the bond strength was significantly affected. The compressive strength of AA-UHPC was further improved by adding more silica fume (SF) to the mixture [14]. The SF content was optimized such that the compressive strength of the cementless AA-UHPC reached that of the conventional UHPC. The decreased W/B due to the flowability improvement by water-reducing admixtures could increase the compressive strength of AA-UHPC.

A comprehensive experimental study was also conducted to investigate the compressive strength and stress–strain relationship of GGBS-based AA-UHPC subjected to various temperatures. The influence of the W/B ratio and steel fiber volume fraction (SF_V) on the mechanical properties of this material was investigated [15]. Regardless of the W/B ratio, the additional steel fibers improved this property, although it was negligible at higher temperatures. The effects of various Ca/Si ratios on the compressive strength of AA-UHPC were studied to achieve the sustainable development of UHPC [16]. The correlation between the compressive strength and Ca/Si ratio is not linear, as there is an optimum value (i.e., 1.2) at which the material's strength increases until it reaches this value and then sharply decreases. The investigation of different silica sand-to-binder (S/B) ratios in the range of 0.16–0.8 was essential to developing a Ca-rich GGBS-based AA-UHPC with a compressive strength greater than 150 MPa [17]. An optimum S/B ratio of 0.8 was achieved, resulting in a compressive strength of 160.7 MPa. The impacts of the precursor component and steel fiber dosage on the compressive strength of AA-UHPC were further examined, leading to the design and proposal of a new environmentally friendly material [18]. It was determined that the optimum value of the SF_V was 2.0%, balancing both the mechanical properties and material costs. In addition, the structural performance of AA-UHPC, incorporating an industrial byproduct with various quantities of sand, was studied using steel and polyethylene fiber reinforcement [19]. The maximum compressive strength of the material was achieved with a 2.0% SF_V and a FA to binder ratio of 0.64. Expanding on these findings, it was observed that the interaction between different materials and their proportions plays a critical role in the overall performance of AA-UHPC. The integration of steel fibers significantly enhances the compressive strength and durability of the composite material [20]. Moreover, the inclusion of industrial byproducts not only contributes to the mechanical properties but also supports the sustainability and cost-effectiveness of the construction materials. The exploration of these parameters is crucial for optimizing the mechanical properties of AA-UHPC and ensuring its applicability in high-performance structural applications.

Although extensive experimental studies have been conducted on the development of cementless AA-UHPC, the experiments have some drawbacks, including time-consuming testing, high labor/material expenses, and a limitation on the number of variables that may be tested. To find precise solutions to such complex difficulties, architectural and civil

engineers have resorted to alternative methodologies, notably computer methods based on artificial intelligence algorithms [21–23]. Abdellatief et al. [24] studied geopolymer UHPC as innovative category of traditional UHPC designed to achieve ultra-high strength and sustainability using different types of machine learning (ML) algorithms to forecast the compressive strength considering 113 experimental tests. Feature importance analysis revealed that steel fiber content and L/B ratio significantly affect compressive strength, while NaOH and silica fume also positively correlate with compressive strength. Extra water and GGBS content, however, showed a low correlation. Key findings reveal that geopolymer UHPC exhibits lower flowability than UHPC, though it remains relatively high, with notably faster setting times. Geopolymer UHPC achieves an early compressive strength of 101 MPa at 7 days, surpassing all UHPCs, and 133 MPa at 28 days, slightly lower than UHPCs, while the production results in significant reductions in CO_2 emissions (up to 70%), embodied energy (up to 73%), and cost (up to 64%) compared to UHPC [25]. Therefore, there is a need to further explore alternative compositions for UHPC to enhance its sustainability and reduce costs while maintaining its superior mechanical properties.

Current data-rich frameworks for anticipatory design can be used to build useful patterns using ML techniques, a well-known subfield of artificial intelligence [26–29]. Several studies have been conducted using ML to predict the material characteristics of UHPC and alkali-activated concrete structures. Five different random forest (RF) ML models were developed to predict the compressive strength of alkali-activated concrete, including blast furnace GGBS and coal FA. A significance analysis of the model was used to evaluate various mix design factors. The compressive strength is primarily affected by the curing age and silicate modulus. A coefficient of determination of 89% was obtained using the proposed model. Similarly, the RF technique was used to predict the compressive strength of FA-based alkali-activated concretes, considering their physiochemical qualities, curing conditions, and mixing processes [30]. The results reveal that the RF model, once properly trained and its hyperparameters rigorously optimized, can generate high-fidelity forecasts for both features of the new AACs. The coefficients of determination (R^2) and mean average error (MAE) were 0.944 and 2.013 MPa, respectively, when predicting the compressive strengths of the materials. Sequential learning has been employed to predict the compressive strength of alkali-activated construction materials containing FA-, and GGBS-based concrete [31]. RF and Gaussian process regressions were implemented separately with the three pipelines, and a comparative study was performed. The performance of the proposed models was outstanding, considering the time required for development and the lower research expenditures.

Accordingly, a comprehensive comparative study was performed using different ML models to predict the compressive strength of AA-UHPC materials. To the best of the authors' knowledge, this study is a pioneering work that considers the application of ML techniques to the important mechanical properties of AA-UHPC materials. This study is a thorough comparative investigation utilizing ML techniques to demonstrate each method's performance and integrate these methods into a stacked model. Twelve model metrics were used and the ML models were scored/ranked based on these indicators. Finally, a graphical user interface (GUI) is proposed for the first time for the convenience of researchers anticipating the target value.

2 Cementless AA-UHPC

According to ASTM C1856 [32], UHPC must have a compressive strength of at least 120 MPa. Thus, cementless AA-UHPC is often composed of tiny powders, aggregates, fibers, and different additives to achieve high compressive strength. As previously stated, AAC is a form of concrete that uses alkali-activated binders rather than OPC to achieve its mechanical properties. The ingredients that can be used in AA-UHPC production are summarized as follows:

- Alkali-activated binders are the main components that provide concrete with strength and durability. These binders are often derived from industrial byproducts, such as FA, GGBS, or other pozzolanic materials that are activated with alkali solutions. Common alkaline activators include sodium silicate (SS) and sodium hydroxide (SH).
- The aggregates are classified as fine or coarse. Fine aggregates may be fine sand or crushed stone, whereas coarse aggregates may be crushed stone or gravel. The aggregates used in concrete can affect its overall strength, density, and workability.
- SF is a byproduct of silicon and ferrosilicon alloy manufacturing. It is frequently used as an additive in AA-UHPC to improve its mechanical quality, reduce porosity, and boost durability.
- Superplasticizers are chemical additives that can be used to increase the workability of concrete while maintaining its strength. This helps lower the W/B ratio while preserving flowability.
- An appropriate curing method is essential for the development of AA-UHPC characteristics. Curing processes such as steam curing and high-pressure curing may be utilized, although the curing temperature is also known to be an effective factor.
- Steel or synthetic fibers have been added to AA-UHPC to increase its ductility and toughness. Depending on

the necessary qualities, steel or synthetic fibers can be employed.

It is crucial to note that the particular formulas and components used in AA-UHPC may vary based on the intended qualities and availability of resources in different regions. Therefore, various factors can affect the compressive strength of AA-UHPC.

3 Research significance

In recent years, alkali activation has been regarded as a viable strategy for producing low-carbon and environmentally friendly construction materials. Owing to the essential global measures toward sustainable designs, high-performance concrete materials will eventually be completely replaced by AA-UHPC because of its superior performance and eco-friendly designs. However, similar to other novel materials, their mechanical properties should be thoroughly investigated. Artificial intelligence has become increasingly popular owing to its outstanding prediction capabilities, which have paved the way for the reduction of labor and material costs. The fewer the experimental tests conducted, the tidier the environment. Having numerous researches on UHPC and AA-UHPC materials, no research has been performed specifically on the prediction of the compressive strength of AA-UHPC materials. Twenty-three ML models were used to estimate target values. Thus, a comprehensive comparative study can be conducted between different ML models. In addition, there is a need to understand the parameters effects on compressive strength of AA-UHPC. Therefore, Shapley diagrams were used to understand the complex correlation between each factor and the output value. Finally, a GUI was proposed to facilitate the prediction process for researchers in this field, as they could provide any input on this interface, obtain the target values, and compare them to their real-world counterparts.

4 Data acquisition and processing

In this research, the steel fiber aspect ratio (SF_A) as one of the critical input features was considered. The aspect ratio refers to the length-to-diameter ratio of the steel fibers used in AA-UHPC. This parameter significantly affects the mechanical performance, and the aim is to capture the influence of fiber geometry on compressive strength of AA-UHPC. From the literature, a data-rich framework was compiled with numerous input factors, including SF_A, SF_V, water content, W/B, sand-to-binder ratio (S/B), FA, silica fume (SF), GGBS, SH, SS, sodium silicate-to-sodium hydroxide ratio (SS/SH), molarity (M), quartz powder content (QP), quartz sand content (QS), sodium metasilicate content (SM), curing temperature (C_T), and curing days (C_D). The output parameter was the compressive strength of AA-UHPC. A literature review of 26 peer-reviewed academic publications [10, 16, 17, 19, 33–54] yielded 284 data points. Table A in the Appendix presents the number of data entries. The statistical characteristics of the datasets are presented in Table 1. Some of the data points were not expressly supplied in the literature; thus, graphs were used with the utmost care. A heatmap of the dataset showing the considered inputs and outputs is shown in Fig. 1. Based on the heatmap with correlation coefficients, "flow" shows a higher correlation with the output (i.e., compressive strength). This is because if the segregation of aggregates is prevented, the mixture with a higher flow is more densely packed in the mold, resulting in higher strength. M, followed by SS/SH, were the next in rank. However, a higher W/B ratio negatively affected the prediction of compressive strength.

Understanding these relationships between input features and compressive strength is essential for predicting and optimizing the performance of AA-UHPC. This comprehensive approach not only enhances the accuracy of predictive models but also provides valuable insights into the material design and optimization for practical applications. SF_A and SF_V are significant as they contribute to the tensile strength and ductility of the AA-UHPC [38–40]. Higher aspect ratios improve the bridging of cracks, enhancing toughness, while an optimal volume of steel fibers boosts the load-bearing capacity and post-cracking behavior, thus contributing to higher compressive strength. Water and W/B are essential for workability and the hydration process. A lower W/B ratio usually results in higher compressive strength due to reduced porosity and enhanced packing density [41–43]. The S/B affects the density and strength of the concrete and an optimal S/B ratio ensures good particle packing, reducing voids and enhancing the mechanical interlock between particles, which contributes to higher compressive strength. FA, SF, and GGBS are supplementary cementitious materials that significantly affect the long-term strength and durability of AA-UHPC. FA improves workability and contributes to long-term strength through pozzolanic reactions [44]. SF enhances matrix density and strength due to its fine particles and high reactivity, while GGBS improves matrix density and strength. The concentrations and ratios of these activators (e.g., SS/SH) directly influence the rate and extent of chemical reactions, thus affecting the compressive strength [45–48]. The QP and QS act as fillers, enhancing packing density and reducing porosity in AA-UHPC [49]. The SM serves as an additional source of silica and improving the mechanical properties of AA-UHPC. Its presence can enhance the matrix's cohesion and overall strength [50]. The C_T and C_D are crucial for the development of mechanical properties; however, the duration of curing ensures the

Table 1 Statistical characteristics of the data points

Feature	Fiber aspect ratio	Fiber volume fraction	Water (kg)	Water/binder	Sand/binder	Flow (mm)	Fly ash (kg)	Silica fume (kg)	GGBS (kg)	Sodium hydroxide (kg)
Mean	50.30	1.07	126.18	0.29	0.87	225.42	18.87	12.25	54.01	5.52
Std	43.12	0.99	107.69	0.10	0.24	81.09	38.14	7.57	22.23	3.90
Min	0.0	0.0	8.40	0.15	0.16	103.0	0.0	1.96	13.01	1.33
25%	0.0	0.0	49.0	0.25	0.75	132.0	0.0	5.5	37.04	3.15
50%	65.0	1.0	97.0	0.30	1.0	244.01	8.39	11.1	50.55	3.88
75%	81.25	2.0	230.0	0.32	1.0	288.75	13.17	18.07	70.0	6.74
Max	125.0	4.0	396.0	1.0	1.0	354.0	172.00	52.67	189.61	14.0

Feature	Sodium silicate(kg)	SS/SH ratio	Molarity	Quartz powder (kg)	Quartz sand (kg)	Sodium metasilicate (kg)	Curing temperature (°C)	Curing days	Compressive strength (MPa)
Mean	21.53	4.99	11.53	13.68	46.10	4.88	29.44	18.66	135.35
Std	23.77	2.32	5.72	7.69	7.30	3.11	17.55	22.53	32.54
Min	0.0	1.50	1.50	7.27	35.22	2.40	17.50	1.0	33.40
25%	10.11	3.00	8.0	8.0	39.35	2.50	20.0	3.0	120.00
50%	15.72	5.16	16.0	10.0	47.94	2.76	23.0	7.0	137.15
75%	23.61	7.00	16.0	18.0	50.0	8.82	25.0	28.0	154.85
Max	175.0	7.73	16.0	39.22	74.20	9.50	90.0	90.0	229.00

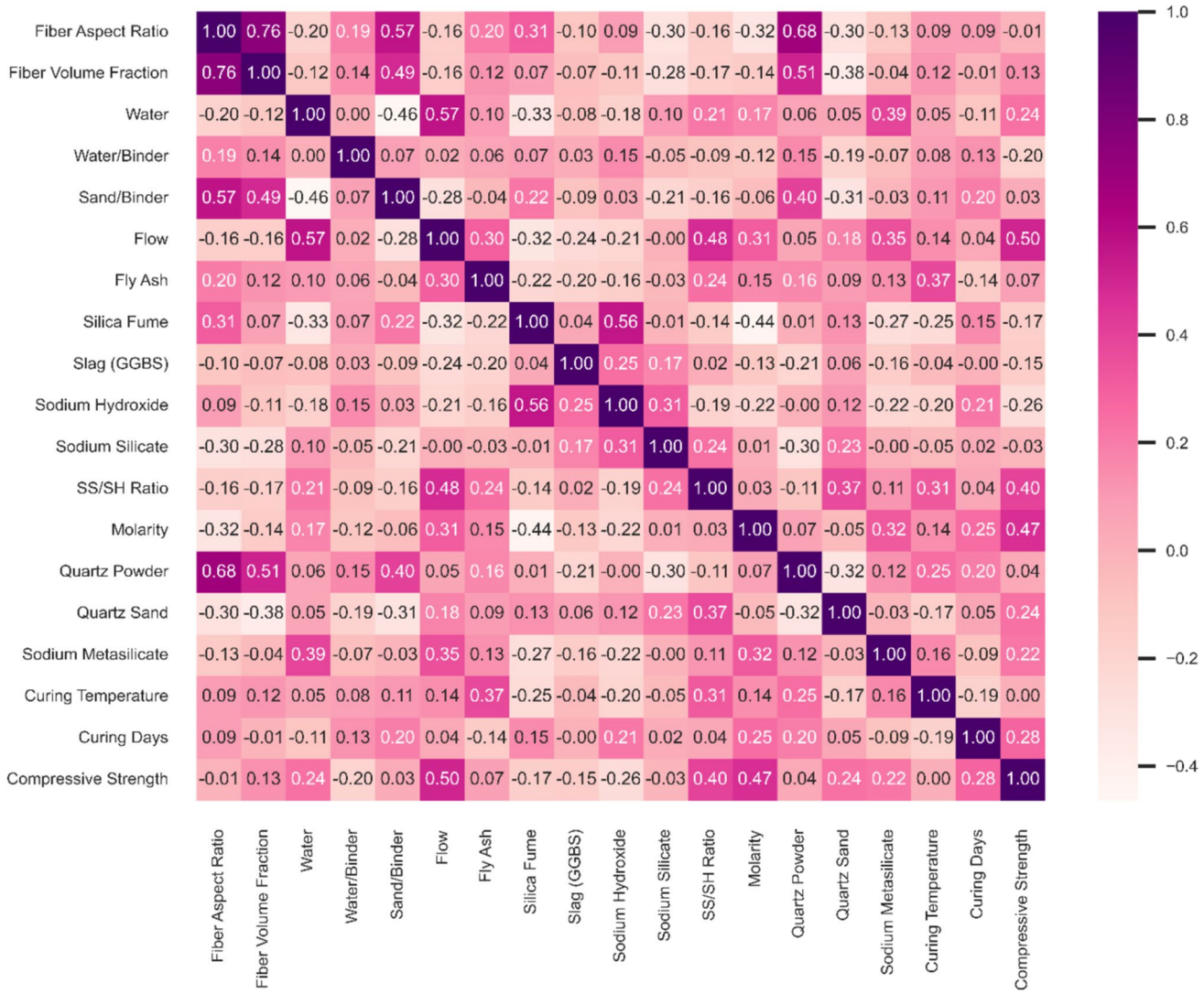

Fig. 1 Heatmap illustration of dataset considered for ML methods

complete reaction of all components, contributing to the development of a dense and strong matrix over time [51–54].

Therefore, a dataset must be curated to verify and improve its quality. Data preparation is the process of modifying or removing useless data prior to use. This is a vital step in the development of ML and data mining algorithms. Many ML techniques require dataset standardization. The dataset framework was preprocessed in two successive stages. MinMaxScaler divides each feature value by its range, which is the difference between the original and minimum values after subtracting the lowest value of that feature. Generally, the MinMaxScaler features have a default range of 0.0 to 1.0. Scale characteristics use statistics that are resistant to outliers, which can negatively affect the mean and variance of the sample. Robust scalers remove the median to decrease fluctuations and scale data to the quantile range, which is the interquartile range (IQR) by default. The IQR was between the 75th and 25th quantiles of the first and third quartiles, respectively. The median and IQR were retained for use in the subsequent data, using the transformation strategy to enhance the results. The outliers, on the other hand, had a negative impact on the sample mean and variance. In such cases, median and interquartile ranges typically yield better results.

4.1 Feature selection and statistical indicators

The purpose of feature selection in ML and data analysis is to select a subset of the relevant characteristics (variables) from the original collection of features. Feature selection was used to improve model performance, reduce overfitting and computing time, and increase model interpretability. Several feature selection techniques have previously been utilized, the three most common of which are the

filter, wrapper, and embedded methods. The filter method evaluates the importance of each feature regardless of the learning algorithm. The wrapper method assesses the performance of a learning algorithm using various feature subsets. The embedded method incorporates feature selection as a part of the model training process. Pearson's correlation coefficient can be determined by:

$$r = \frac{\sum (x_i - \bar{x})(y_i - \bar{y})}{\sqrt{\sum (x_i - \bar{x})^2 (y_i - \bar{y})^2}} \quad (1)$$

where r,$\bar{x}$,x_i, $\bar{y}$, and y_i are the Pearson coefficient, mean of variable x, x, mean of variable y, and y, respectively.

Various techniques, known as model metrics, have been utilized to evaluate precision of ML models. They indicate accuracy of predictions provided by an ML model subjected to various conditions within a test dataset. Twelve model metrics were used to provide a level of compatibility with the ML algorithms for predicting the target values in this study, as listed in Table 2.

4.2 Shapley additive exPlanations

The Shapley additive exPlanations (SHAP) values can be used to evaluate the significance of various aspects of a model. The premise for calculating feature significance is the change in the inaccuracy of a certain disturbance prediction. This is a visualization tool that can be used to visually represent the output of an ML model to make it easier to understand. The goal of SHAP is to explain the prediction of instance X by estimating the contribution of each characteristic to the prediction. Coalitional game theory was used to determine the Shapley values using the SHAP technique. The Shapley values demonstrate how to divide the predictions evenly across the characteristics. SHAP is determined by:

$$\varphi_k(val) = \sum_{s \subseteq N \setminus \{i\}} \frac{|s|!(n - |s| - 1)!}{n!} (val(s \cup \{i\}) - val(s)) \quad (2)$$

wherein feature importance showed by *val*, which is the weighted summation n features assuming i vector of the

Table 2 Twelve statistical indicators used in this study [55]

Formula	Description
$R^2 = 1 - \frac{\sum_{i=1}^{n} (\text{Actual}_i - \text{Predicted}_i)^2}{\sum_{i=1}^{n} (\text{Actual}_i - \text{Actual}_{avg})^2}$	Coefficient of determination
$MSE = \frac{1}{n} \sum_{i=1}^{n} \left(\text{Actual}_i - \text{Predicted}_i\right)^2$	Mean squared error
$RMSE = \sqrt{\frac{1}{n} \sum_{i=1}^{n} \left(\text{Actual}_i - \text{Predicted}_i\right)^2}$	Root mean squared error
$MAE = \frac{1}{n} \sum_{i=1}^{n} \left\lvert \text{Actual}_i - \text{Predicted}_i \right\rvert$	Mean absolute error
$MARE = \frac{1}{n} \sum_{i=1}^{n} \left\lvert \frac{\text{Actual}_i - \text{Predicted}_i}{\text{Actual}_i} \right\rvert$	Mean absolute relative error
$MSRE = \frac{1}{n} \sum_{i=1}^{n} \left\lvert \frac{\text{Actual}_i - \text{Predicted}_i}{\text{Actual}_i} \right\rvert^2$	Mean square relative error
$RMSRE = \sqrt{\frac{1}{n} \sum_{i=1}^{n} \left(\frac{\text{Actual}_i - \text{Predicted}_i}{\text{Actual}_i} \right)^2}$	Root mean squared relative error
$RRMSE = \frac{\sqrt{\frac{1}{n} \sum_{i=1}^{n} (\text{Actual}_i - \text{Predicted}_i)^2}}{\sum_{i=1}^{n} \text{Actual}_i} \times 100$	Relative root mean square error
$MBE = \frac{1}{n} \sum_{i=1}^{n} \left(\text{Actual}_i - \text{Predicted}_i\right)$	Mean bias error
$\text{erMAX} = \max \left(\left\lvert \frac{\text{Actual}_i - \text{Predicted}_i}{\text{Actual}_i} \right\rvert \right)$	Maximum absolute relative error
$\text{SD} = \sqrt{\frac{\sum (X_i - \text{Arithmetic mean})^2}{\text{total number}}}$	Standard deviation of the difference between actual and predicted values
$U_{95} = \sqrt{1.96(SD^2 + RMSE^2)}$	Uncertainty at 95%

feature values. Assuming s as subset of model features, $s!(n-|s|-1)!n!$ can be known as weight and $val(s)$ is its predicted value. However, the sum of SHAP features and standard features can be target of model:

$$g(x) = l(x_s) = \varphi_0 + \sum_{t=1}^{n} \varphi_t x_s^i \tag{3}$$

where φ_0 is the standard feature value, φ_t is the SHAP feature, and x_s is vector for input variables.

5 Machine learning methods

The three primary divisions of the ML approach are reinforcement, supervised learning, and unsupervised learning. As described in further detail in this section, 19 enhanced ML models were used to make the predictions. The following are important descriptions of the ML models used in this study.

5.1 Tree-based methods

To determine the category or value of the target variable, "tree-based" models, a subset of supervised ML, identify attributes and build a tree-like structure. The ensemble approach of the RF methodology employs bootstrap aggregation to generate decision trees. The prediction criteria were developed using a nonparametric regression approach, and explicit prior knowledge of the predictor and output coupling was not required. The compilation of all the generated decision tree predictions is the final output of the algorithm. This method allows for approximately equal consideration of all data dimensions and avoids substantial tree linkages.

The RF is a complex assembly algorithm that employs various decision trees as principal predictors. One advantage of this model is a reduced number of model variables, which reduces the possibility of overfitting. In this method, a decision tree is utilized as the building block. It provides numerous decision tree algorithms using different feature spaces and training datasets. Averaging is then used to combine the individual models to obtain the final results. A bagging regressor (BR) is used through different repeats to provide an aggregated predictor. Aggregation employs a plurality vote when anticipating a class and the average across variations when predicting numerical targets. Creating bootstrap clones and using them as a new training set result in numerous training set iterations. Subset selection in linear regression and classification trees can be used to improve the accuracy of real datasets. The built predictor can be significantly altered when the learning set is disrupted. As a result, BR can increase the anticipation performance. The constructed predictor can change significantly when the training set is shuffled. Therefore, prediction performance can be enhanced through BR. The extra tree regression (ETR) tool is a synchronous learning model that constructs randomly selected decision trees.

A more sophisticated iteration of the ETR method, the extremely randomized tree regressor (ERTR), adopts a random decision tree choice strategy that reduces the error function. ERTR is a decision-tree-based ML technique that generates a set of decision trees without pruning them into a top-to-bottom style of tree growth. ERTR constructs a set of decision trees in the same manner as other tree-based ensemble techniques, but with an emphasis on adding randomization to decrease variance without excessively enhancing bias. It is an instance-based simple learning method that performs predictions by locating the k-nearest data points to a given input, then averaging their target values to forecast a new input. In the k-nearest neighbor (KNN) model, "k" refers to the number of nearest neighbors (data points) considered to make a prediction for a new data point. KNN is a non-parametric and laundry learning method that makes no assumptions about the underlying data distribution and does not learn an explicit model during training [56–58].

The main difference between these models lies in the level of randomness introduced during tree construction. ETR and ERTR introduce more randomness than RF, which, in turn, introduces more randomness than BR. The increased randomness in ETR and ERTR tends to reduce model variance, making them less likely than RF to overfit noisy data. However, this extra randomness may also slightly increase bias. BR, while reducing the variance, like RF, can be applied to various base models, offering flexibility. RF, ETR, and ERTR employ bootstrapped samples and feature subsets to enhance diversity in the ensemble. In contrast, BR focuses mainly on bootstrapped samples.

5.2 Boosting algorithms

By combining weak learners as strong learner, the ensemble learning technique known as "boosting" can improve the performance of weak learners. The primary goal of boosting is to improve weak learners through iterative training, emphasizing instances that were previously misclassified or difficult to predict. Boosting algorithms can concentrate on challenging cases and gradually enhance their performance through adaptive learning processes. The fundamental theoretical idea of the AdaBoost algorithm, which is an iterative model, is to achieve a weak classifier by iteratively learning the same dataset and then combining the various weak classifiers gained during training to obtain a strong classifier.

New trees are introduced into the boosting operation to minimize the inaccuracy of predicting target variables in the boosting approach. The estimation error is reduced by adding a new tree to the gradient boosting machine (GBM)

structure with a constant learning factor until the model achieved its maximum feasible accuracy [59]. The precision and speed of gradient boosting for execution can be enhanced by randomly subsampling the training data to prevent overfitting. LightGBM (LGBM) is a novel gradient-boosting decision-tree model that handles large datasets with numerous characteristics. It incorporates gradient-based one-sided sampling and unique feature bundling techniques to improve training while retaining model accuracy and performance. The histogram-based GBM (HGBM) approach separates continuous information into discrete bins. A histogram-based technique can save processing time and memory by creating attribute histograms rather than seeking split points. When addressing regression problems, the main principle of Extreme Gradient Boosting (XGBoost) is to employ a greedy technique to learn each base tree. The residual inaccuracy between the predicted and true values is continually minimized by constantly creating new decision trees to fit the residuals of the previous anticipation, thereby improving the prediction precision. CatBoost is a new gradient-boosting algorithm that can handle categorical features with minimal loss. This algorithm possesses several specific characteristics compared with different gradient boosting models, such that during the model training process, a set of decision trees is constructed successively to modify the gradient bias of each subsequent tree. The key advantage of this model is the efficient processing and ranking enhancement of category attributes [60].

Techniques such as regularization (L_1/L_2) are present in XGBoost and LightGBM, which can help prevent overfitting. AdaBoost does not inherently include regularization. CatBoost is specifically designed for categorical-feature handling, making it a strong choice when dealing with such features, whereas other models require additional preprocessing. LightGBM and CatBoost were optimized for efficiency, making them suitable for large datasets. In addition, XGBoost and LightGBM are known for their efficient parallel processing, which makes them suitable for multicore systems**.** LightGBM and CatBoost often consume less memory than the other models, which can be beneficial when working in resource-constrained environments. CatBoost often requires less parameter tuning and can provide a competitive performance with minimal hyperparameter adjustments.

5.3 Neural networks

The structure and operation of neural networks in the human brain serve as the basis for a computer model known as a neural network. This is a crucial component of both contemporary deep learning and ML. The artificial neural networks (ANNs) algorithm was designed to effectively detect correlations between input variables and determine significant interactions between them. An ANNs model typically comprises an input layer that feeds the input parameters, a hidden neuron layer that processes the input parameters, and a final output layer that provides the output results. Furthermore, the hidden layer has functions that specify weights for each variable, which aids in determining the amount of reliance of various inputs on one another for an accurate intended output result. Echo state networks (ESNs) are efficient in handling temporal data and are gaining popularity owing to their simple training, strong performance in time-series prediction, and clear architecture with input, reservoir, and output layers. ESNs adhere to the "echo state property," which means that only readout weights are trained, leaving reservoir weights constant and preserving reservoir dynamics. Radial basis function networks (RBFNs) excel in function approximation and pattern identification and are ideal for interpolation, classification, and regression. These use radial basis functions as activation functions to capture complex nonlinear correlations. The RBFNs training involves centroid selection, width adjustment, and weight learning. Recurrent neural networks (RNNs) specialize in sequential data, such as time series and videos. With cyclic connections, RNNs remember previous information and dynamically process consecutive inputs, which makes them suitable for tasks involving sequences [61, 62].

ESNs and RNNs are explicitly designed for temporal data and handle sequences efficiently, whereas RBFNs focus on function approximation and pattern identification. ESNs have a simple training process, which consists primarily of adjusting the readout weights, whereas RBFNs and RNNs may involve more complex training steps, such as centroid selection and handling cyclic connections. RNNs, due to their cyclic connections, have inherent memories that allow them to remember previous inputs, whereas ESNs and RBFNs do not possess this built-in memory feature. ESNs have a distinct reservoir layer, whereas RBFNs use radial basis functions and RNNs incorporate cyclic connections, making them specialized for sequential data. ESNs are popular for time-series prediction, RBFNs for function approximation, and RNNs for handling sequential data, including time series. Because the selection of the right model depends on the nature of the data and the specific task, all models were employed and investigated in this study.

5.4 Data selection technique

Leave-one-out and *k*-fold cross-validations have been extensively used as model preparation criteria. Both methods require building models with a subset of data while saving another subset, known as hold-out fold, for model validation. Conventionally, hyperparameter optimization is accomplished by grid search, which entails examining full hyperparameter space of training method. When working with

parameter spaces that contain actual or unbounded values, a grid search allows the user to establish bounds.

Missing values are ubiquitous in real-world datasets and may cause problems for ML algorithms that demand complete data. As the data points in Appendix Table A had missing values, the ML algorithms could be simply coded to predict the outputs based on the input attributes. During analysis, the ML algorithms required comparable input properties. SimpleImputer and KNNImputer were used to solve the missing data problem by providing simple and effective methods for handling missing values in a dataset. The SimpleImputer class provides a simple method for addressing missing values by replacing them with predefined strategies or values. It can be applied to both numerical and categorical data and operates on a feature or column basis.

SimpleImputer provides a simple and adaptable method for handling missing data by replacing them with logical values based on a predefined strategy. The KNNImputer class estimates missing values using the nearest-neighbor methodology, considering the KNN technique values for each sample with missing features. Based on the given characteristics, it determines the k closest samples and uses their non-missing values to impute the missing values. KNNImputer computes the distances based on both numerical and categorical information. To impute the missing values, it employs the mean value for numerical characteristics and the most common value for categorical features.

5.5 Hyperparameter optimization

The optimization of hyperparameters is a critical stage in the creation of ML models. Hyperparameters are configurations in which the model cannot be learned during training. However, they determine how the learning process works and how the model behaves. The learning rate, number of layers in the neural network, number of hidden units, regularization strength, and batch size are all examples of hyperparameters. The purpose of hyperparameter optimization is to determine the optimum combination of hyperparameter values that maximizes the ML model's performance on a particular task. The procedure involves experimenting with various hyperparameter setups and assessing their effects on the model's performance.

There are various methods for optimizing hyperparameters, including grid search, random search, Bayesian, gradient-based, or particle swarm optimization, and genetic algorithms. Caution must be employed when using hyperparameter optimization techniques because they are frequently computationally expensive and time-consuming, particularly for complicated models and huge datasets. When determining the optimization approach to apply, the balance between exploration and utilization should be struck, and account computing restrictions must be considered. Hyperopt and tuning are examples of automated hyperparameter optimization libraries that can be used to simplify and streamline hyperparameter tuning in various ML frameworks [57, 62].

5.6 Active learning method

Active learning in ML is a specialized approach that optimizes model training by iteratively selecting and labeling the most informative instances from a pool of unlabeled data. Unlike traditional supervised learning where all labeled data are used upfront, active learning strategically chooses which data points to label, focusing on those that are most beneficial for model improvement. The iterative nature of active learning involves a user who assists in labeling selected instances, directing the model to learn from the most critical samples. By actively seeking information from the unlabeled dataset, active learning aims to enhance model performance using fewer labeled instances, ultimately reducing labeling costs and computational resources while maximizing predictive accuracy. The process typically revolves around query strategies that intelligently select samples for labeling, such as uncertainty sampling, query by committee, expected model change, among others. These strategies guide the model to select instances that exhibit ambiguity or uncertainty, thereby refining its understanding of complex patterns in the data. Through iterative cycles of model training, querying, and updating, active learning continually refines the model's knowledge, adapting and optimizing its predictive capabilities. This methodology finds applications in various domains where labeling large datasets is expensive, time-consuming, or impractical, enabling efficient utilization of resources while achieving superior model performance. Active learning is typically integrated into the training phase of each individual base model within the ensemble. During active learning, the focus is on selecting the most informative or uncertain instances from the unlabeled data pool and then using those instances to update or fine-tune the individual models.

5.7 Stacked ML model by active learning methodology

Although there are many ML methods that can be used for different types of engineering problems, the Stacked ML model, which is a logical combination of ML methods, is a powerful tool for employing the best ML models and their aggregation results. Figure 2 illustrates four types of Stacked ML models used in this study in order of their highest prediction accuracy, which were improved with active learning method. The procedure for constructing a Stacked ML model involves several interconnected steps. Initially, individual ML models are trained using diverse algorithms on the training dataset. Active learning is applied to each base

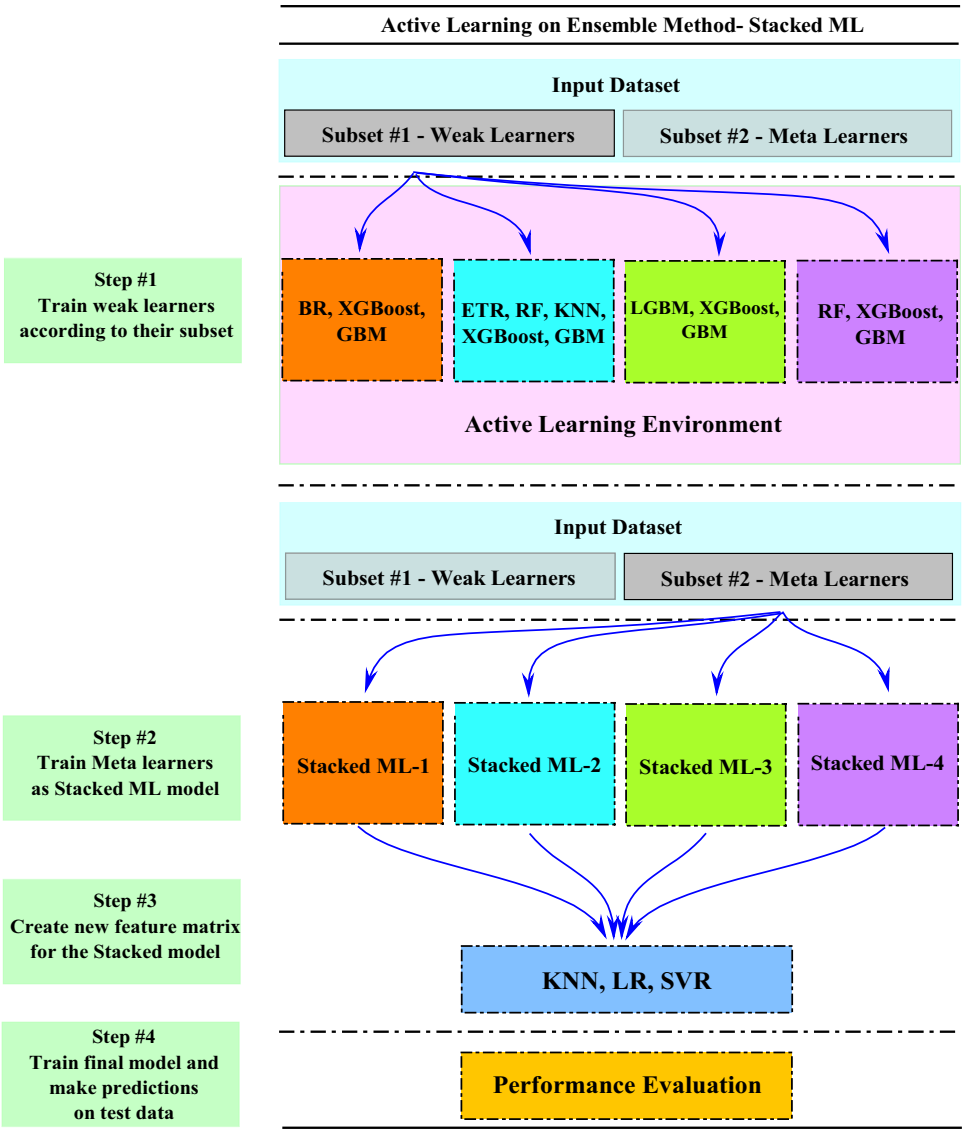

Fig. 2 Architecture of the optimized Stacked ML models with active learning method

model within the ensemble. It involves selecting instances from the pool of unlabeled data and using them to improve each base model's understanding of the data. Once the individual models have been updated through active learning, their predictions can be combined or aggregated in a way that best leverages the strengths of each model to make a final prediction. This aggregation step often occurs after the active learning process has updated the base models. Subsequently, predictions were generated for the test data using individual models. These predictions were then combined to form a new feature matrix that served as the input for the final Stacked ML model. This ultimate model, often a linear regression (LR) or support vector regression (SVR), is trained using an aggregated feature matrix. After training, a stacked model was employed to predict the outcomes of the test dataset using the generated stacked features. The final phase involves evaluating the performance of the Stacked ML model, which is typically accomplished by examining various performance metrics such as the statistical indicators presented in Table 2. This comprehensive sequence of steps culminates in the establishment of a powerful Stacked ML model that combines the strengths of individual models to enhance overall predictive capabilities.

The Stacked ML algorithm proposed herein incorporates aforementioned feature selection methods to eliminate redundant input features from the dataset. In addition, hyperparameters were optimized using the optimization algorithm implemented in Tree-based Pipeline Optimization Tool (TPOT), a Python AutoML (Automated ML) provided by AutoSklearn. Figure 3 shows automated TPOT process, where the shadowed part depicts the automated step. Employing the TPOT enhances solutions for optimizing ML pipelines within proposed Stacked ML models. Consequently, effectiveness of proposed Stacked ML algorithm

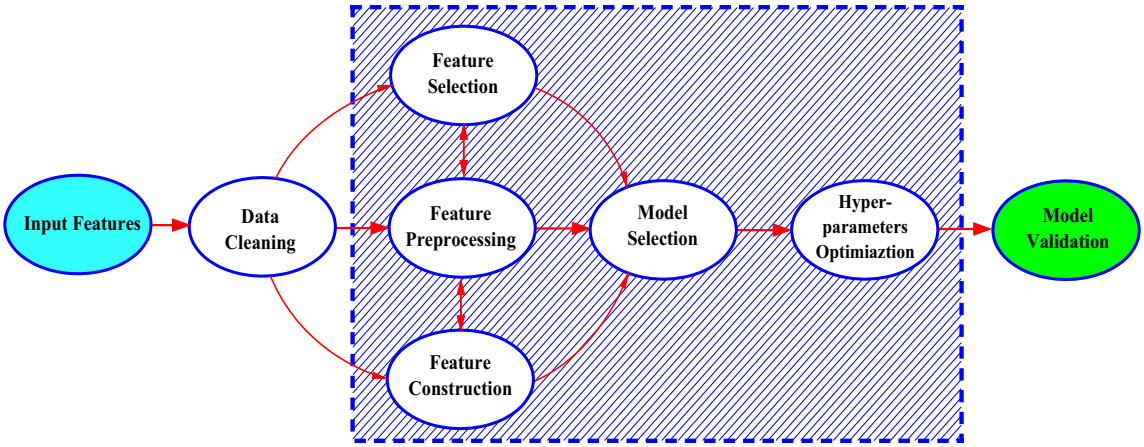

Fig. 3 Tree-based Pipeline Optimization Tool

Table 3 Results of hyperparameters optimization for the Stacked ML models

Random state	Max depth	Min split	Min leaf	Learning rate	Estimators	Sub Models
–	8	10	20	0.01	4000	XGBoost
–	6	10	15	0.001	2500	GBM
–	6	–	–	0.01	1500	LGBM
2	–	8	10	–	600	ETR
0	–	–	–	–	800	BR
1	8	–	–	–	800	RF

was assessed on the dataset, and the most efficient sub-models are highlighted in Table 3. Notably, the sub-models utilized for Stacked ML algorithm were optimized to enhance results and reduce execution time [62].

6 Data preprocessing and feature selection

6.1 SHAP evaluations

The Shapley values for a series of query points were calculated to evaluate input parameter effects on prediction of the compressive strength of AA-UHPC. The mean SHAP value with the average impact on the model is shown in Fig. 4. Note that Fig. 4 considers the absolute SHAP value; hence, it is irrelevant whether the characteristic has a positive or negative effect on prediction. The most important features for predicting the target parameters were the flow, SH, curing days, water, and molarity. The effect of flow, an important parameter, was approximately two times greater than that of morality. The number of SH and curing days had a similar effect on predicting compressive strength of AA-UHPC, considering their importance. By contrast, S/B, SF, SM, and QS were among the variables with the least importance in the prediction of target values. By utilizing SHAP

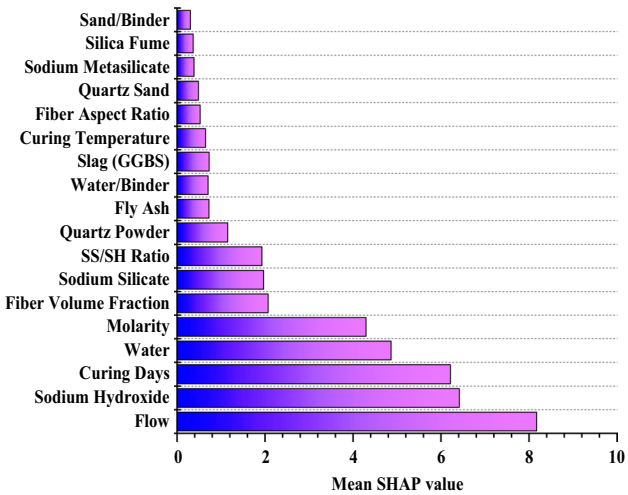

Fig. 4 SHAP global interpretation on compressive strength of AA-UHPC, mean SHAP value with average impact on model

to create a beeswarm plot, as shown in Fig. 5, it was possible to further analyze the impact of changes in various feature values on the model target. The input parameters are shown on the y-axis in ascending order of significance. The input parameter values are used to determine the blue (low) and

Fig. 5 SHAP global interpretation on compressive strength of AA-UHPC, SHAP value impact on the model

red (high) dots. The data density provides information on the amount of information dispersed at a certain location. The higher the value of the flow, the more positive the impact on the compressive strength of AA-UHPC. Interestingly, SH has a negative effect on the output value because higher values of this variable lead to lower prediction values of the target value. For the curing days, no definite conclusion could be reached; generally, lower values of this parameter resulted in lower predicted values for the target parameter. In addition, the SF_V and SS/SH ratio increased the corresponding SHAP values and led to higher target prediction values.

The decision-making process followed by each prediction is illustrated in Fig. 6. Individual data instances can be followed up and evaluated using this type of analysis. The plotted data were used to compute the relevance of each feature, which was then used to arrange the features by default. Each line on the top of the graph meets the x-axis at the expected value for its associated observation, which determines the color of the line on the spectrum. The SHAP value for each feature was added to the base value of the model as the graph moved from bottom to top. This illustrates the effect of each element on the overall prediction. The waterfall chart expects a single row of an explanation object as the input because it is designed to show explanations for specific forecasts. Figure 7 shows the SHAP waterfall plot. The average predicted compressive strength was 136.189 MPa, as

Fig. 6 SHAP decision model

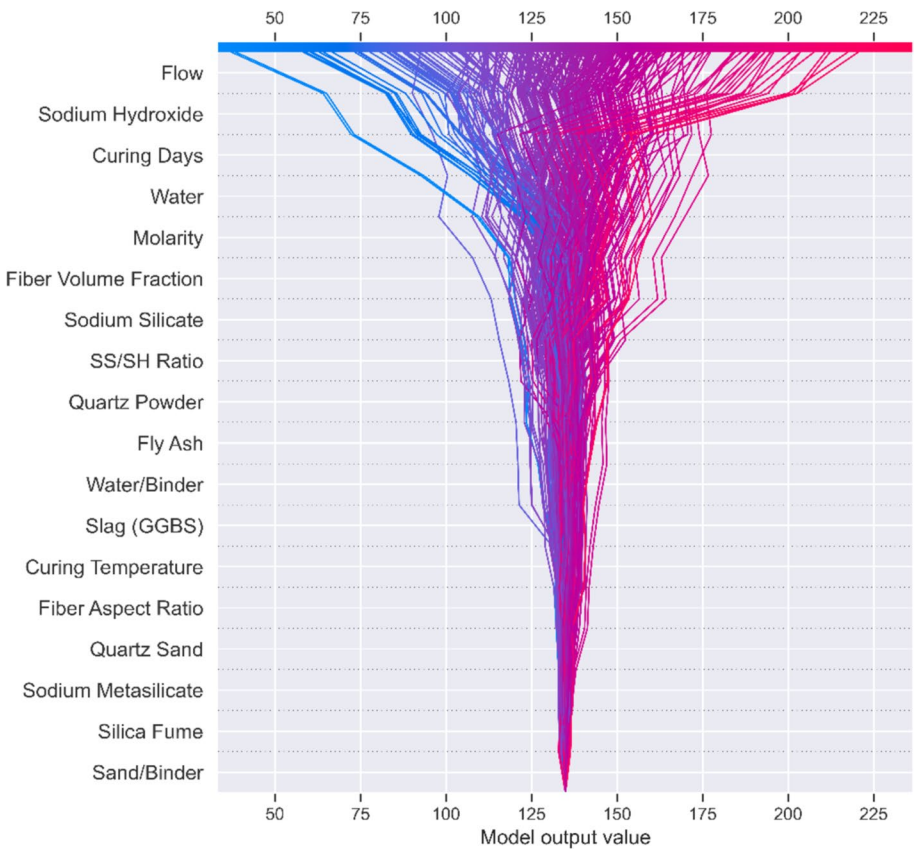

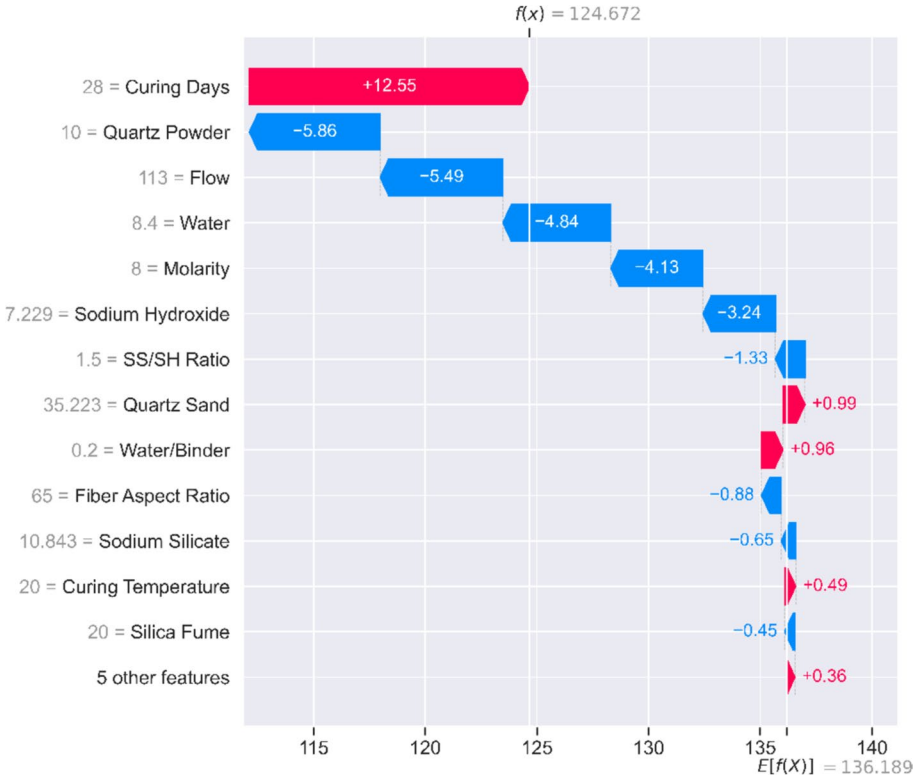

Fig. 7 SHAP waterfall explainer of input features

indicated by the gray color of *E [f(x)]*. The gray colors on the vertical axis correspond to the input feature values. Red represents the enhancement of the predicted target values, whereas blue corresponds to a reduction in the predicted output parameter. For example, a curing day with a value of 28 pulled the predicted target value higher by 12.55. Flow, with a value of 113, on the other hand, pushed the predicted compressive strength lower with a value of 5.49. These representations can be interpreted for other input features using a waterfall SHAP diagram.

6.2 Partial dependence plot

The partial dependence plot (PDP) illustrates the marginal influence of one input feature on the total prediction of the ML model. Therefore, it is possible to determine the relationship between the target and selected features in terms of linearity, fluctuation, or complexity. To better evaluate the effect of each feature, the PDP of all the input features are plotted in Fig. 8. The two features, SF and C_T, showed a linear behavior, whereas SF_A and S/B had similar behaviors for predicting the compressive strength of AA-UHPC. In contrast, the features W, SF_V, M, SS/SH ratio, and C_D showed an ever-increasing trend, confirming their increasing effect on the prediction of the target. In contrast, SH, SS, FA, and W/B exhibited decreasing trends in the estimation of compressive strength. Although most of the features had a direct effect on the target, some features, such as flow, QP, QS, and SM, fluctuated in the PDP plot. Therefore, they may have different effects on the target based on their values. In addition, the input features of water, flow, SH, W/B, and C_D have the most significant effect on the target and cannot be neglected during predictions, whereas the other features can be neglected.

7 Results and discussion

7.1 Prediction of concrete compressive strength using ML methods

In this section, the results of the ML model are presented. After careful evaluation of the features and important parameters that affect the results of the ML methods, training and testing datasets were prepared for use in the ML algorithms. Figure 9 illustrates the scatter of actual and predicted values of the compressive strength of AA-UHPC under curing conditions of 1, 3, 7, 14, 28, and 90 days. The ML models of LGBM, GBM, AdaBoost, BR, ETR, and RF, with accuracy percentages of 92.6%, 91.9%, 91.8%, 0.907%, 90.1%, and 90%, respectively, provided the best estimations of the compressive strength of AA-UHPC. Moreover, the XGBoost, ERTR, RNNs, ESNs, RBFNs, HGBM, and CatBoost models had accuracies of 89.4% and 83.6%, respectively, while the ANNs and KNN had accuracies of 74.5% and 71.3%, respectively. Figure 10

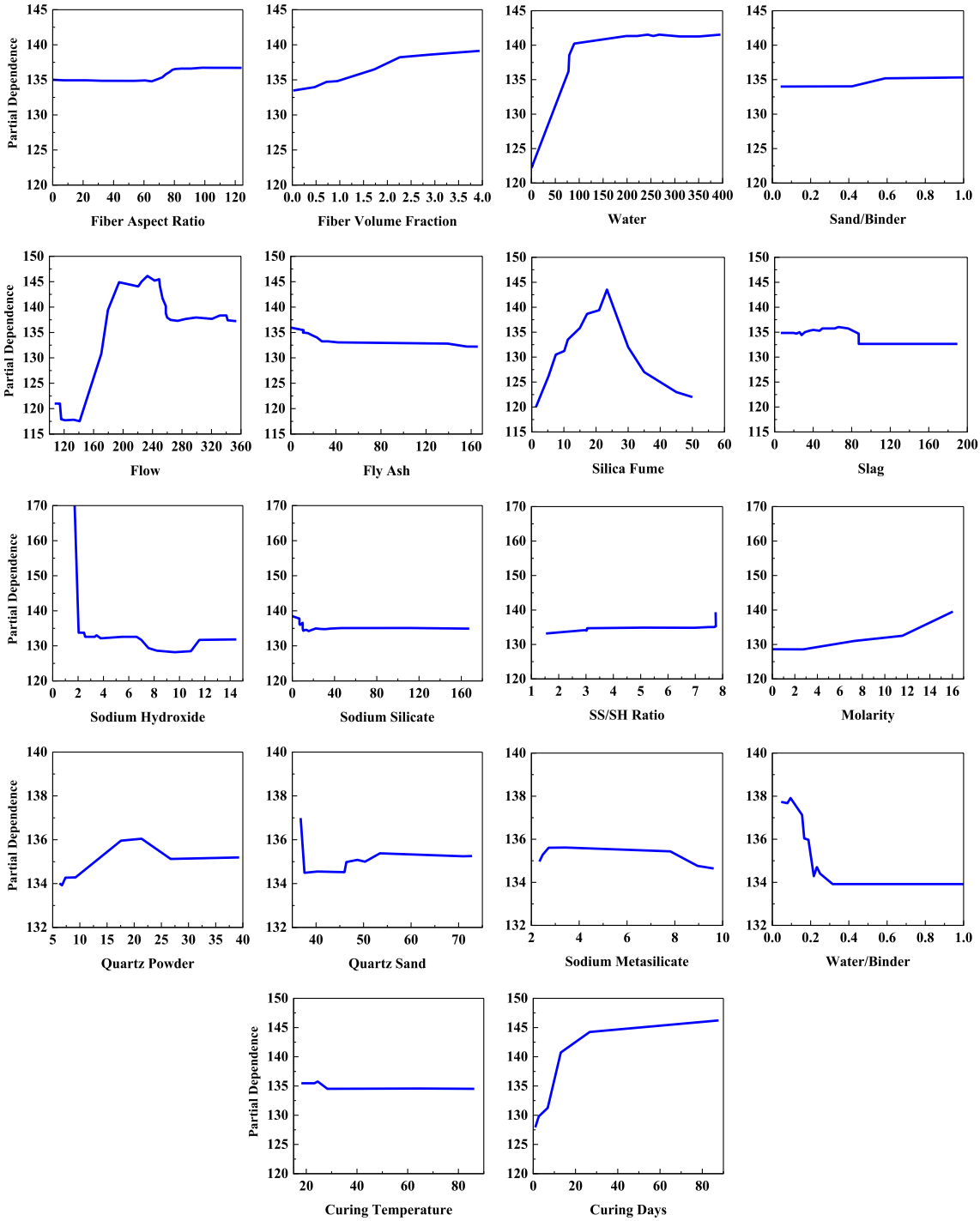

Fig. 8 Partial dependence plot of input features

illustrates the error values of the ML models, in which the closer the bar graphs are to zero, the higher the accuracy of the ML models. Therefore, the AdaBoost, ETR, XGBoost, and CatBoost models had better error values than the other methods. Interestingly, none of the neural network-based models could accurately predict the output value, as the scattered points were not evenly distributed near the X = Y line.

Although ML models can estimate the compressive strength of AA-UHPC with more than 90% accuracy, these methods are simplified for implementation, and the results may vary with dataset changes. Stacked ML models have

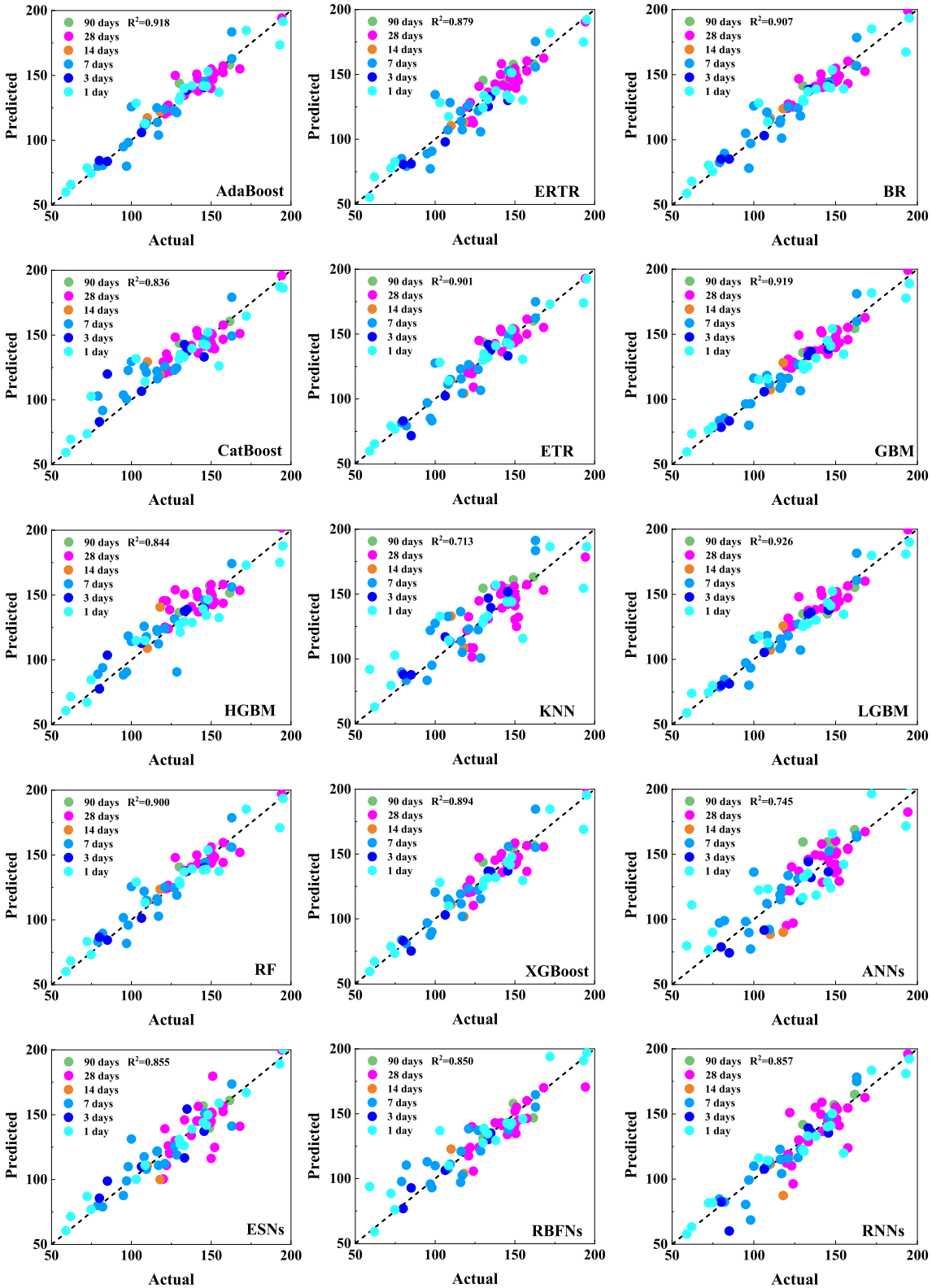

Fig. 9 Results of predictions of concrete compressive strength considering the curing day using ML algorithms

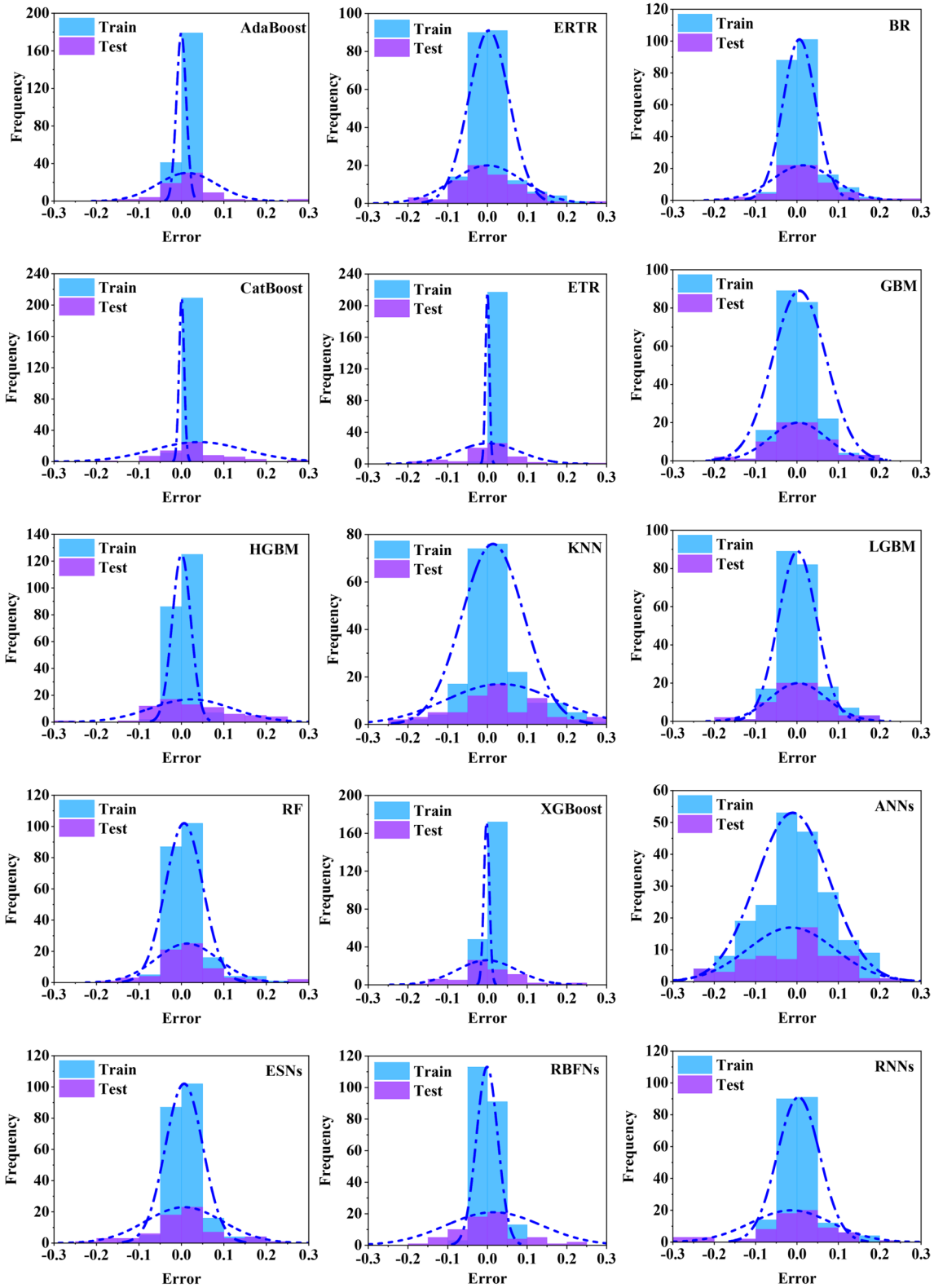

Fig. 10 Results of error values of the ML algorithms

been introduced to overcome the shortcomings of ML models. According to definition of Stacked ML models in Sect. 5.6, results of four Stacked ML models are shown in Fig. 11. Stacked ML-3, Stacked ML-1, Stacked ML-4, and Stacked ML-1 had prediction accuracies of 93.2%, 91.9%, 91.8%, and 90.5%, respectively. More importantly, compared to the error values of the ML models presented in Fig. 10, the error values of the Stacked ML model presented in Fig. 12 confirm the capability of the proposed models to predict the compressive strength of AA-UHPC considering different curing days.

Since 12 evaluation indicators were used, score marker method was considered to present the performance of ML models for estimating the compressive strength of AA-UHPC. A score marker is a comprehensive assessment tool used to evaluate and compare different entities based on the statistical indicators listed in Table 2. These indicators provide quantitative measures of performance, and the score marker assigns scores to each entity based on their performance. The key feature of a score marker is that it not only considers the individual scores in each indicator but also considers the trend of these scores, both ascending and descending, providing a more balanced evaluation. Once the scores for all indicators and trends were determined for each entity, the total score was calculated, enabling a direct comparison among the entities. Table 4 lists the score markers for the test dataset. These scores allow for a direct comparison among entities, highlighting their relative strengths and weaknesses. ML models with lower total scores are generally considered to perform better across the selected indicators, and trend analysis provides additional context by considering whether the performance is improving or deteriorating. The results of the score marker can be used for various purposes, such as benchmarking, performance evaluation, resource allocation, ranking, and decision-making. It provides a structured and quantitative approach for comparing ML models, helping civil engineers make informed choices based on objective data. In general, a score lower than 70 indicates the best values that can be achieved by the ML models. Therefore, the Stacked ML-3, LGBM, Stacked ML-1, Stacked ML-4, AdaBoost, and Stacked ML-2 models with scores of 17, 34, 48, 60, 65, and 71, respectively, were selected as the best prediction models. In contrast, the ESNs, CatBoost, RBFNs, RNNs, KNNs, and ANNs models, with scores of 160, 179, 179, 182, 207, and 208, respectively, had the lowest values, which means that their predictions are inaccurate.

7.2 Active learning on Stacked ML models

In this section, effects of implementing active learning on Stacked ML models have been explored. Since the Stacked ML models have the best performance among those ML models investigated in Table 4, they are improved with active learning method to investigate the capability of active learning methodology. Figure 13 illustrates the active

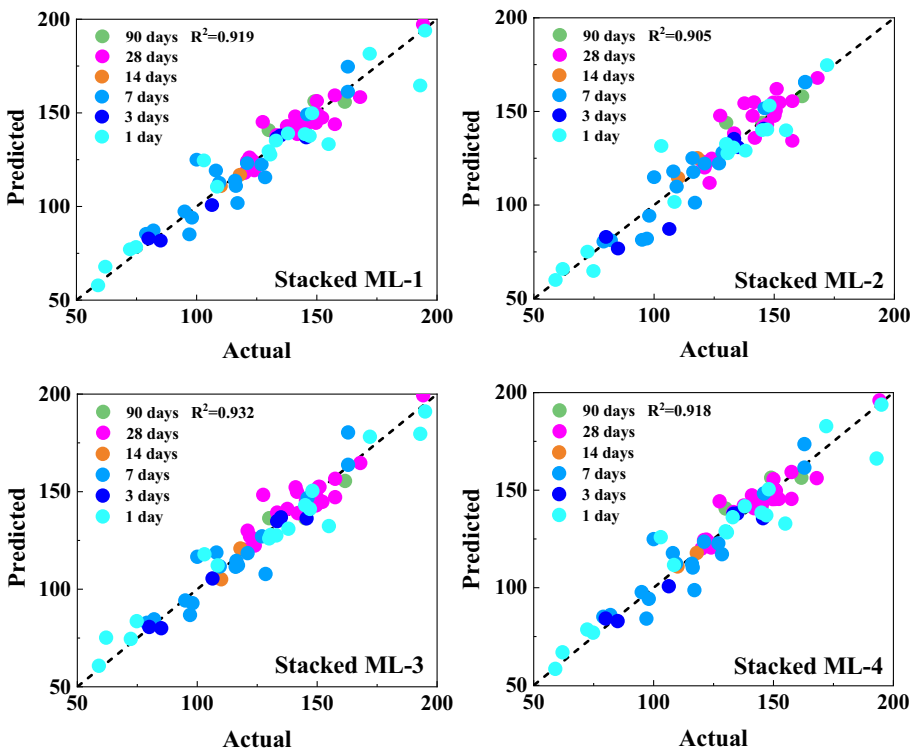

Fig. 11 Results of predictions of concrete compressive strength considering the curing day using Stacked ML algorithms

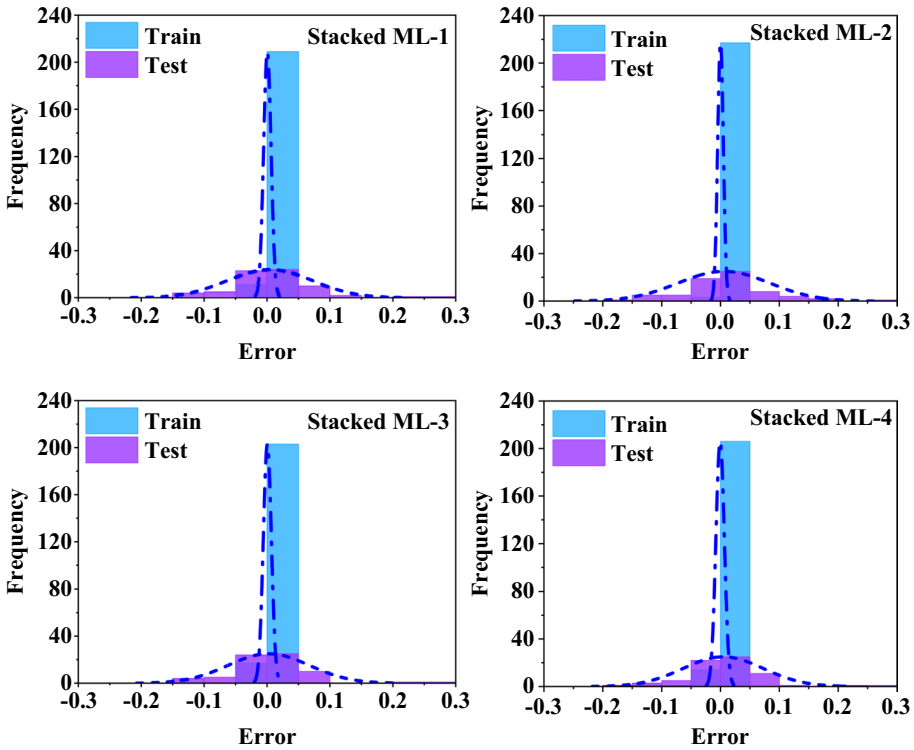

Fig. 12 Results of error values of the Stacked ML algorithms

Table 4 Statistical indicators for estimating compressive strength of test dataset

Model	R^2	MSE	RMSE	MAE	MARE	MSRE	RMSRE	RRMSE	MBE	erMAX	SD	U_{95}	Score
RF	0.900	86.84	9.32	6.94	0.053	0.006	0.074	0.096	0.959	0.256	8.82	25.15	97
LGBM	0.926	63.80	7.99	6.05	0.048	0.004	0.066	0.088	−0.583	0.193	8.02	22.19	34
XGBoost	0.894	92.07	9.60	7.15	0.056	0.006	0.075	0.106	−0.611	0.245	9.65	26.67	110
BR	0.907	80.42	8.97	6.62	0.053	0.006	0.075	0.098	1.118	0.260	8.96	24.85	99
ETR	0.901	85.52	9.25	6.68	0.055	0.006	0.078	0.102	−0.143	0.276	9.31	25.72	102
CatBoost	0.836	142.02	11.92	8.41	0.074	0.013	0.115	0.128	3.365	0.411	11.51	32.48	179
GBM	0.919	69.82	8.36	6.51	0.162	0.060	0.244	0.231	5.139	0.892	21.36	44.95	166
HGBM	0.844	134.98	11.62	9.13	0.052	0.005	0.068	0.092	−0.292	0.188	8.41	28.11	93
AdaBoost	0.918	71.22	8.44	5.79	0.046	0.005	0.069	0.092	1.247	0.258	8.41	23.35	65
KNN	0.713	248.73	15.77	12.04	0.10	0.020	0.141	0.170	2.451	0.559	15.69	43.61	207
ERTR	0.879	105.32	10.26	7.78	0.064	0.008	0.088	0.113	−0.495	0.344	10.32	28.53	142
ANNs	0.745	196.81	18.23	15.36	0.107	0.025	0.157	0.168	0.734	0.792	15.49	46.88	208
ESNs	0.855	152.40	13.50	17.36	0.065	0.008	0.091	0.125	−0.010	0.313	11.44	34.69	160
RBFNs	0.850	181.26	12.20	18.89	0.073	0.014	0.119	0.126	0.373	0.591	11.52	32.90	179
RNNs	0.857	183.07	17.19	14.08	0.069	0.010	0.099	0.134	−1.883	0.30	11.91	40.99	182
Stacked ML-1	0.919	70.17	8.38	5.99	0.048	0.005	0.067	0.092	0.0	0.250	8.44	23.30	48
Stacked ML-2	0.905	94.25	9.71	6.97	0.056	0.006	0.078	0.106	0.985	0.277	9.73	26.94	71
Stacked ML-3	0.932	59.19	7.69	5.69	0.046	0.004	0.065	0.085	0.0	0.213	7.75	21.40	17
Stacked ML-4	0.918	70.65	8.41	5.94	0.048	0.005	0.068	0.093	0.0	0.249	8.47	23.38	60

learning Stacked ML algorithms used for predicting concrete compressive strength, considering the curing day. It can be observed that AL-Stacked ML-1, AL-Stacked ML-2, AL-Stacked ML-3, and AL-Stacked ML-4, with accuracies of 95.9%, 96.8%, 98.1%, and 94.5%, respectively, outperformed the Stacked ML models. Results confirm the ability of active learning methodology on improving the prediction accuracy. Moreover, the error values have been reduced accordingly

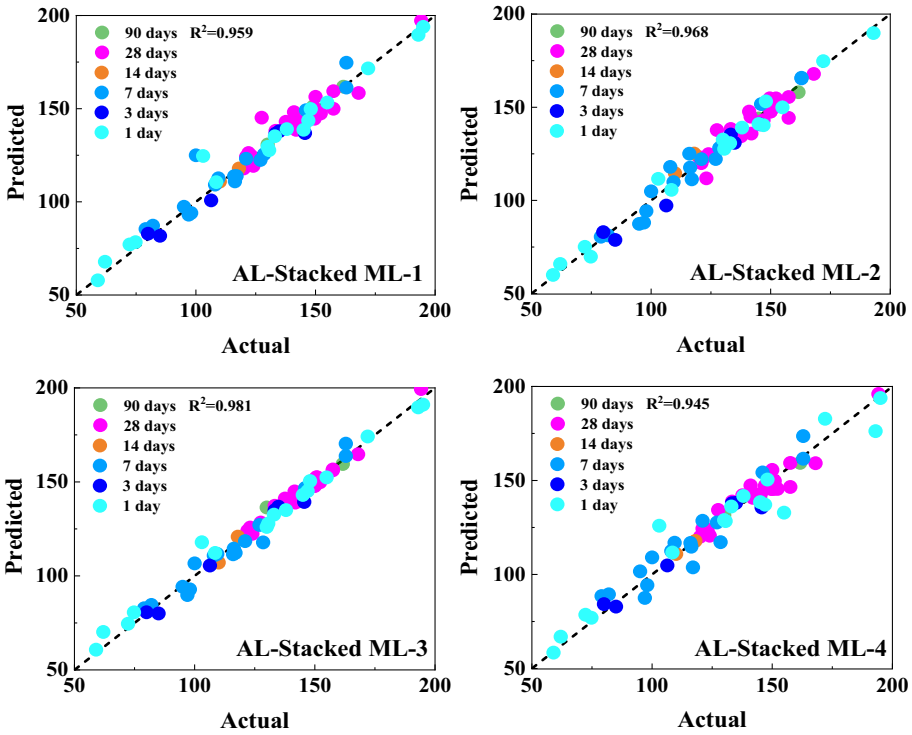

Fig. 13 Active learning Stacked ML algorithms used for predicting concrete compressive strength considering the curing day

and led to have more reliable predication models. Therefore, active learning method has been implemented on Stacked ML models for providing a general estimation model.

8 Validation of estimation models for general experimental test

In this section, a general dataset was selected to validate the proposed ML model. Notably, the selected experimental specimens have not been used before and are categorized as unseen datasets. Therefore, the experimental specimens investigated by Liu et al. [63] were considered. The input features and associated compressive strengths are listed in Table 5. The details of the experimental test and sample preparation are provided by Liu et al. [63]. The data extracted from this study served as a benchmark for assessing the accuracy and reliability of the predictive models and methodologies utilized in this research. This validation process not only ensured the robustness of the proposed ML models but also established a solid foundation for the application of AA-UHPC in practical engineering scenarios, enhancing the credibility of the results and conclusions derived from this study.

All the developed models were validated for an unseen dataset, and the results of the assessment are presented in Table 6. The capabilities of the ML algorithms were improved based on the training and testing datasets described in the previous section. To cover a general target, Stacked ML models were introduced as a complete model to obtain

Table 5 Experimental data for validating the prediction models [63]

l/d	SF_V	W (kg)	W/B	S/B	F (mm)	FA (kg)	SF (kg)	GGBS (kg)	SH (kg)	SS (kg)	SS/SH	M	C_T (℃)	C_D (d)	F_C (MPa)
67	1	97	0.32	1	250.06	12.63	3.3	50.55	3.3	23.07	7	1.5	80	28	142.1
67	2	97	0.32	1	245.0	12.63	3.3	50.55	3.3	23.07	7	1.5	80	28	158.9
67	3	97	0.32	1	229.04	12.63	3.3	50.55	3.3	23.07	7	1.5	80	28	168.5
108	1	97	0.32	1	255.1	12.63	3.3	50.55	3.3	23.07	7	1.5	80	28	145.9
108	2	97	0.32	1	247.06	12.63	3.3	50.55	3.3	23.07	7	1.5	80	28	161.6
108	3	97	0.32	1	230.12	12.63	3.3	50.55	3.3	23.07	7	1.5	80	28	170.4
65	1	97	0.32	1	255.1	12.63	3.3	50.55	3.3	23.07	7	1.5	80	28	131.5
65	2	97	0.32	1	247.06	12.63	3.3	50.55	3.3	23.07	7	1.5	80	28	141.6
65	3	97	0.32	1	240.1	12.63	3.3	50.55	3.3	23.07	7	1.5	80	28	150.8

Table 6 Statistical indicators for estimating compressive strength of experimental test

Model	R^2	MSE	RMSE	MAE	MARE	MSRE	RMSRE	RRMSE	MBE	erMAX	SD	U_{95}	Score
RF	0.855	51.39	7.17	6.30	0.040	0.002	0.045	0.539	−4.50	0.070	5.92	18.23	108
LGBM	0.806	44.69	6.68	6.17	0.040	0.002	0.043	0.496	−2.74	0.075	6.47	18.23	240
XGBoost	0.817	33.30	5.77	4.69	0.031	0.001	0.037	0.426	−1.82	0.065	5.81	16.05	204
BR	0.850	53.32	7.30	6.51	0.042	0.002	0.046	0.548	−4.38	0.070	6.20	18.77	132
ETR	0.823	38.45	6.20	5.13	0.034	0.002	0.040	0.460	−2.68	0.080	5.93	16.82	180
CatBoost	0.747	72.89	8.54	7.13	0.046	0.003	0.053	0.644	−5.13	0.104	7.24	21.94	276
GBM	0.752	62.44	7.90	6.55	0.043	0.003	0.050	0.595	−4.77	0.113	6.68	20.28	264
HGBM	0.822	45.08	6.71	5.88	0.037	0.002	0.042	0.500	−3.13	0.070	6.30	18.05	192
AdaBoost	0.825	30.82	5.55	4.91	0.032	0.001	0.037	0.409	−1.46	0.062	5.68	15.57	168
KNN	0.851	80.96	9.00	7.68	0.050	0.003	0.057	0.691	−7.59	0.084	5.13	20.30	120
ERTR	0.806	49.85	7.06	6.05	0.040	0.002	0.046	0.524	−2.58	0.080	6.97	19.44	252
ANNs	0.817	38.15	6.18	5.70	0.038	0.002	0.041	0.458	−2.55	0.064	5.97	16.83	216
ESNs	0.811	110.63	10.52	9.29	0.063	0.005	0.072	0.809	−7.97	0.134	7.28	25.07	228
RBFNs	0.827	38.74	6.22	5.56	0.037	0.002	0.042	0.463	−2.84	0.082	5.87	16.77	156
RNNs	0.836	83.18	9.12	7.58	0.051	0.004	0.064	0.634	7.58	0.130	5.38	20.75	144
Stacked ML-1	0.921	12.56	3.54	3.05	0.021	0.001	0.025	0.258	0.50	0.040	3.72	10.07	84
Stacked ML-2	0.925	21.44	4.63	3.05	0.019	0.001	0.028	0.344	−2.83	0.062	3.89	11.85	72
Stacked ML-3	0.961	6.22	2.49	2.15	0.014	0.001	0.016	0.182	−0.16	0.025	2.64	7.12	36
Stacked ML-4	0.901	15.57	3.95	3.40	0.023	0.001	0.027	0.287	0.18	0.046	4.18	11.27	96
AL-Stacked ML-1	0.945	9.16	2.89	2.45	0.016	0.001	0.015	0.163	−0.15	0.027	3.42	6.79	48
AL-Stacked ML-2	0.963	5.97	2.45	2.07	0.013	0.001	0.014	0.175	−0.14	0.021	2.58	7.03	24
AL-Stacked ML-3	0.989	4.78	2.13	2.01	0.011	0.001	0.011	0.111	−0.09	0.013	2.01	5.03	12
AL-Stacked ML-4	0.931	11.36	3.04	2.68	0.017	0.001	0.018	0.179	−0.43	0.032	3.65	8.52	60

results from the methods and choose the best predictions. The results of score markers revealed that Stacked ML-3, Stacked ML-2, Stacked ML-1, and Stacked ML-4, with scores of 36, 72, 84, and 96, respectively, had the best estimations of the compressive strength of AA-UHPC. While adding the active learning ability to these models improved their scores to 12, 24, 48, and 60, respectively (i.e., AL-Stacked ML-3, AL-Stacked ML-2, AL-Stacked ML-1, and AL-Stacked ML-4). Therefore, they were selected as the best methods and used for implementation in the GUI.

To further evaluate and compare ML models, Taylor diagram was utilized in Fig. 14 for predicting the compressive strength of AA-UHPC. Taylor diagram is a graphical tool used to assess and compare the performance of predictive models by visualizing multiple statistical metrics simultaneously, such as R^2, RMSE, and standard deviation. In the diagram, the position of each model is indicated relative to the observed data, with ideal models clustering closer to the reference point, which represents perfect correlation and minimal error. This provides a clear, comprehensive view of each model's performance and helps identify the most accurate and reliable models for practical applications. According to Taylor's diagram, proposed Stacked ML models can estimate the compressive strength of AA-UHPC with higher alignment with observed data compared to conventional ML models (Fig. 14a–c). However, the diagram showed that the AL-Stacked ML models consistently achieved better alignment with observed data, demonstrating improved accuracy and reliability compared to their non-active learning Stacked ML models (Fig. 14d). Consequently, the AL-Stacked ML models were selected as the most effective methods and integrated into the GUI for practical application.

9 Graphical user interface

A GUI was developed to predict the compressive strength of AA-UHPC with the ability to plot compressive strength against the number of curing days and predict the strength for each curing day, which is a significant advancement in civil engineering. This intuitive tool combines the power of computational modeling with user-friendly visualization, offering engineers, researchers, and practitioners a streamlined approach for predicting the compressive strength of AA-UHPC while significantly reducing the reliance on extensive experimental testing and computational efforts. The need for such a GUI diminishes the need for extensive experimental testing, thereby saving time and resources and increasing overall efficiency in the development and application of AA-UHPC.

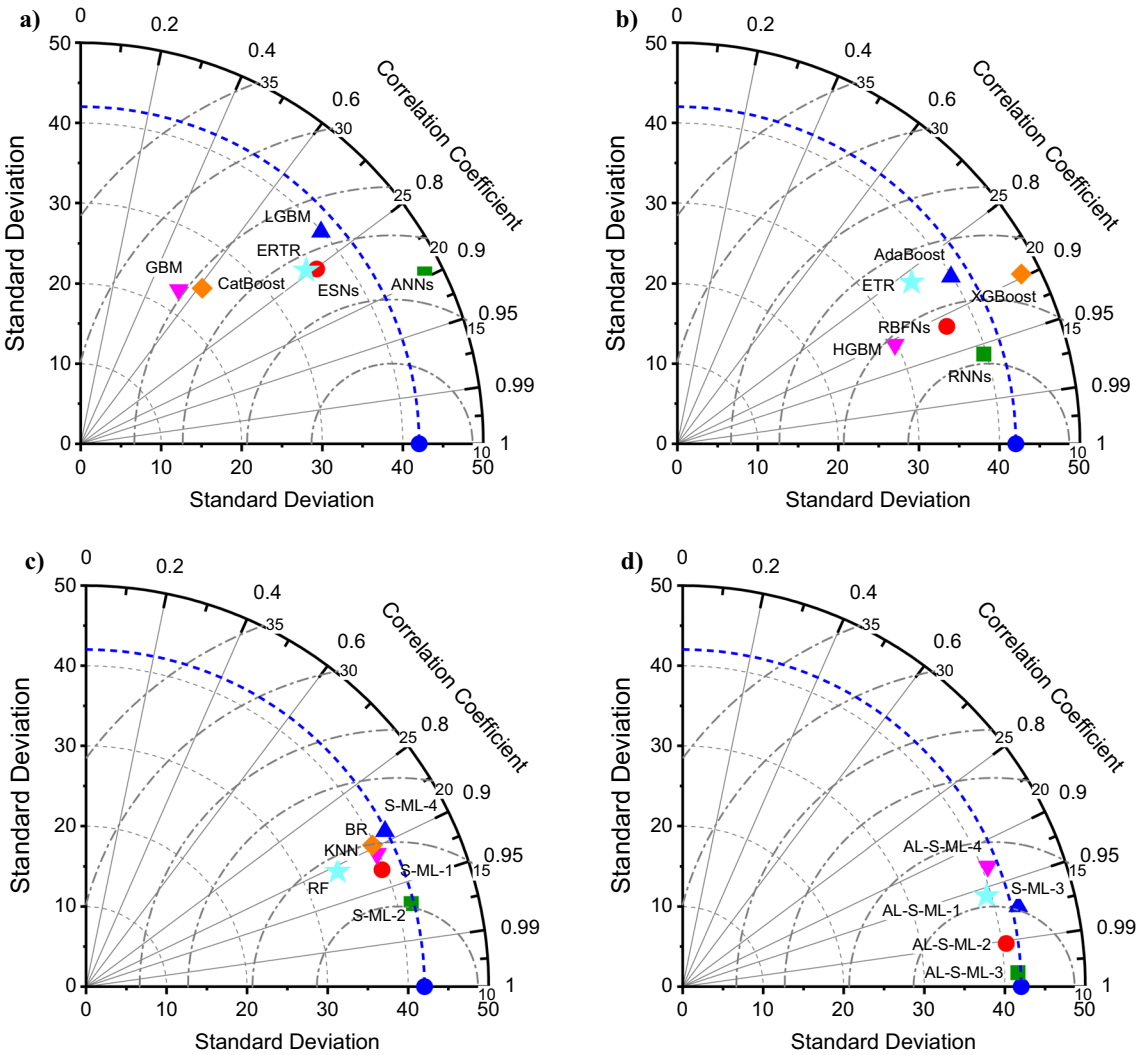

Fig. 14 Taylor diagram for proposed ML models for predicting compressive strength of AA-UHPC

To validate the GUI, the experimental test has been conducted on six cubic specimens having 50 mm dimensions and different ratios of the FA, SF_V, SS, SH, S/B, and GGBS. Figure 15 presents compressive strength test of specimens according to ASTM C109 [64]. The compressive strength of the specimens has been used to validate the use of GUI and its ability to predict the compressive strength according to input parameters. Then the GUI has been developed and has been used to predict compressive strength of AA-UHPC according to input parameters presented. Figure 16 illustrates capability of GUI for predicting compressive strength of AA-UHPC having different input features and curing days.

AA-UHPC, one of the most environmentally friendly construction materials, requires extensive testing to assess its mechanical properties, particularly its compressive strength. Traditional methods involve fabricating and testing physical samples, a process that requires considerable time and resources and is cost-prohibitive. Furthermore, the process can be influenced by various factors, including sample preparation, curing conditions, and testing procedures, which may introduce experimental errors. The GUI offers an alternative approach that minimizes the reliance on labor-intensive and time-consuming procedures, thereby contributing to more efficient concrete research and development. The ability of the GUI to predict compressive strength against curing days has immense value. Accurate prediction models based on empirical data and the proposed Stacked ML models were integrated into the GUI. This enables users to input the curing time, and the GUI instantly generates an estimated compressive strength value, thereby eliminating the need to wait until end of curing period for experimental results. Engineers and researchers can quickly assess the potential strength of AA-UHPC at different stages of the

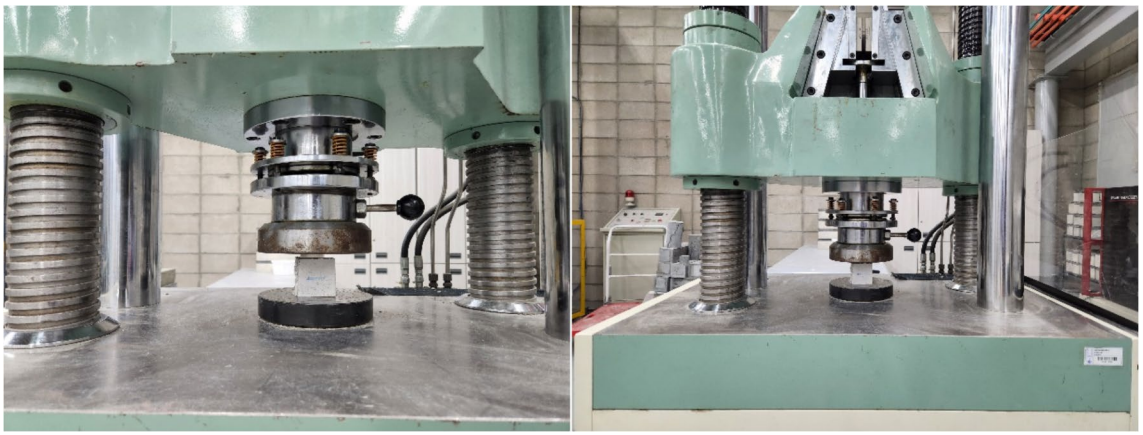

Fig. 15 Compressive strength test of AA-UHPC

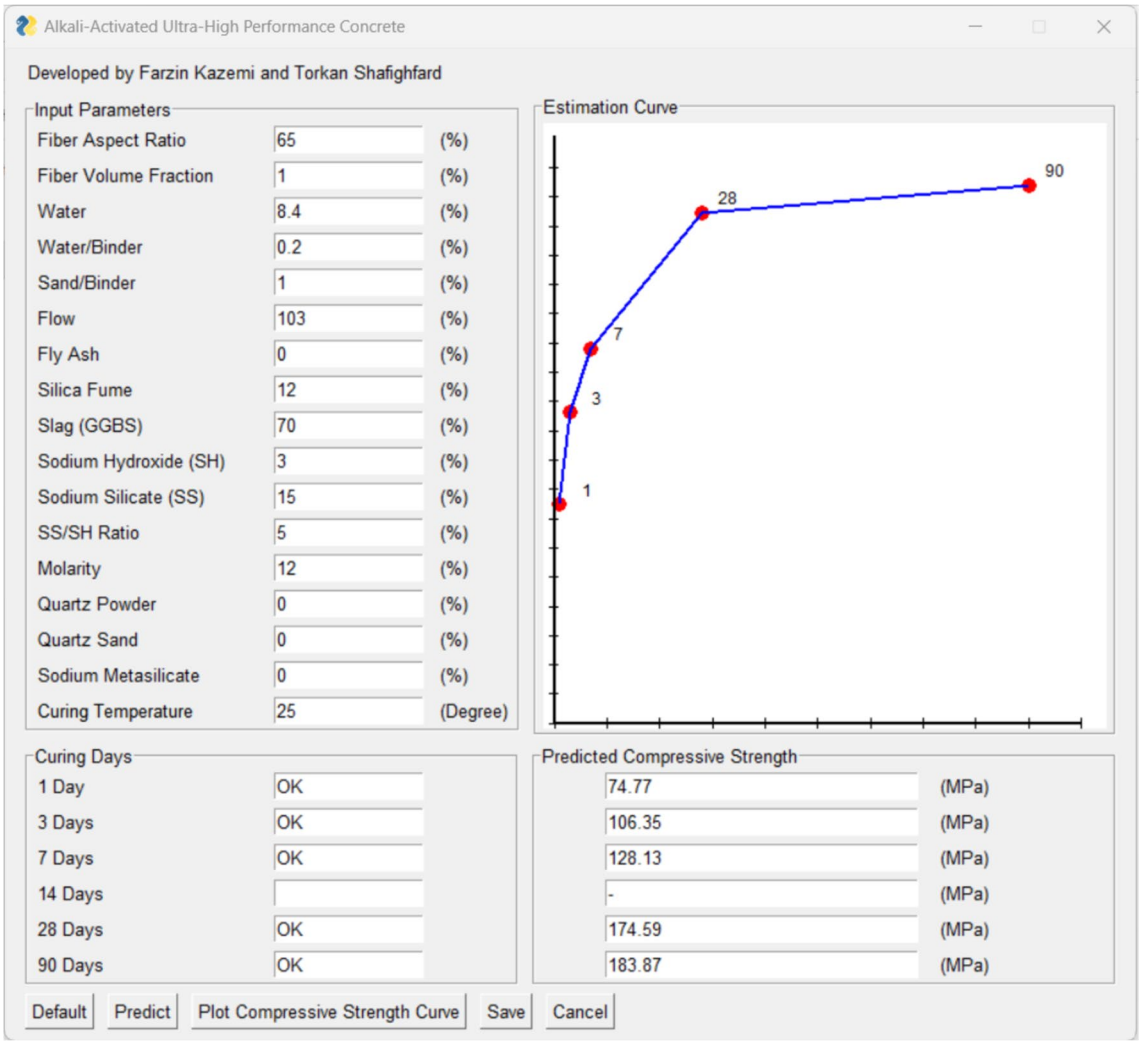

Fig. 16 GUI for predicting compressive strength of AA-UHPC in different curing days (will be available and updated at https://github.com/FarzinKazemi)

Table 7 Data points of experimental tests used for training and testing ML method

l/d	SF_V	W (kg)	W/B	S/B	F (mm)	FA (kg)	SF (kg)	GGBS (kg)	SH (kg)	SS (kg)	SS/SH	M	QP (kg)	QS (kg)	SM (kg)	C_T (°C)	C_D (Days)	FC ((MPa)	Refs.
0.00	0.00	–	0.20	–	–	0.00	12.00	70.00	–	–	–	–	18.00	–	2.50	25.00	1.00	74.40	[33]
65.00	1.00	–	0.20	–	–	0.00	12.00	70.00	–	–	–	–	18.00	–	2.50	25.00	1.00	74.80	[33]
0.00	0.00	–	0.20	–	–	0.00	12.00	70.00	–	–	–	–	18.00	–	2.50	25.00	3.00	108.20	[33]
65.00	1.00	–	0.20	–	–	0.00	12.00	70.00	–	–	–	–	18.00	–	2.50	25.00	3.00	106.40	[33]
0.00	0.00	–	0.20	–	–	0.00	12.00	70.00	–	–	–	–	18.00	–	2.50	25.00	7.00	128.50	[33]
65.00	1.00	–	0.20	–	–	0.00	12.00	70.00	–	–	–	–	18.00	–	2.50	25.00	7.00	128.10	[33]
0.00	0.00	–	0.20	–	–	0.00	12.00	70.00	–	–	–	–	18.00	–	2.50	25.00	28.00	161.90	[33]
65.00	1.00	–	0.20	–	–	0.00	12.00	70.00	–	–	–	–	18.00	–	2.50	25.00	28.00	174.60	[33]
0.00	0.00	–	0.20	–	–	0.00	12.00	70.00	–	–	–	–	18.00	–	2.50	25.00	90.00	155.40	[33]
0.00	0.00	–	0.20	–	–	0.00	12.00	70.00	–	–	–	–	18.00	–	2.50	25.00	90.00	173.90	[33]
65.00	1.50	–	0.30	1.00	–	0.00	20.00	70.00	–	–	–	–	10.00	–	2.40	20.00	3.00	82.20	[34]
65.00	1.00	–	0.20	1.00	–	0.00	20.00	70.00	–	–	–	–	10.00	–	2.40	20.00	3.00	82.50	[34]
65.00	1.50	–	0.20	1.00	–	0.00	20.00	70.00	–	–	–	–	10.00	–	2.40	20.00	3.00	83.70	[34]
65.00	1.50	–	0.30	1.00	–	0.00	20.00	70.00	–	–	–	–	10.00	–	2.40	20.00	7.00	96.90	[34]
65.00	1.00	–	0.20	1.00	–	0.00	20.00	70.00	–	–	–	–	10.00	–	2.40	20.00	7.00	103.30	[34]
65.00	1.50	–	0.20	1.00	–	0.00	20.00	70.00	–	–	–	–	10.00	–	2.40	20.00	7.00	101.70	[34]
65.00	1.50	–	0.30	1.00	–	0.00	20.00	70.00	–	–	–	–	10.00	–	2.40	20.00	14.00	103.80	[34]
65.00	1.00	–	0.20	1.00	–	0.00	20.00	70.00	–	–	–	–	10.00	–	2.40	20.00	14.00	120.20	[34]
65.00	1.50	–	0.20	1.00	–	0.00	20.00	70.00	–	–	–	–	10.00	–	2.40	20.00	14.00	117.40	[34]
65.00	1.50	–	0.30	1.00	–	0.00	20.00	70.00	–	–	–	–	10.00	–	2.40	20.00	28.00	119.90	[34]
65.00	1.00	–	0.20	1.00	–	0.00	20.00	70.00	–	–	–	–	10.00	–	2.40	20.00	28.00	124.20	[34]
65.00	1.50	–	0.20	1.00	–	0.00	20.00	70.00	–	–	–	–	10.00	-	2.40	20.00	28.00	129.10	[34]
65.00	2.00	–	0.30	0.80	–	20.00	5.00	75.00	–	–	–	–	–	–	–	17.50	3.00	85.00	[10]
65.00	2.00	–	0.30	0.80	–	20.00	5.00	75.00	–	–	–	–	–	–	–	90.00	3.00	120.00	[10]
65.00	2.00	–	0.30	0.80	–	20.00	5.00	75.00	–	–	–	–	–	–	–	17.50	7.00	98.00	[10]
65.00	2.00	–	0.30	0.80	–	20.00	5.00	75.00	–	–	–	–	–	–	–	90.00	7.00	130.00	[10]
65.00	2.00	–	0.30	0.80	–	20.00	5.00	75.00	–	–	–	–	–	–	–	17.50	28.00	122.00	[10]
65.00	2.00	–	0.30	0.80	–	20.00	5.00	75.00	–	–	–	–	–	–	–	90.00	28.00	151.00	[10]
0.00	0.00	–	0.30	–	–	0.00	20.00	70.00	–	–	–	–	10.00	–	–	23.00	3.00	83.00	[35]
0.00	0.00	–	0.20	–	–	0.00	20.00	70.00	–	–	–	–	10.00	–	–	23.00	3.00	93.00	[35]
0.00	0.00	–	0.30	–	–	0.00	20.00	70.00	–	–	–	–	10.00	–	–	23.00	3.00	80.00	[35]
0.00	0.00	–	0.30	–	–	0.00	20.00	70.00	–	–	–	–	10.00	–	–	23.00	7.00	102.00	[35]
0.00	0.00	–	0.20	–	–	0.00	20.00	70.00	–	–	–	–	10.00	–	–	23.00	7.00	117.00	[35]
0.00	0.00	–	0.30	–	–	0.00	20.00	70.00	–	–	–	–	10.00	–	–	23.00	7.00	108.00	[35]
0.00	0.00	–	0.30	–	–	0.00	20.00	70.00	–	–	–	–	10.00	–	–	23.00	28.00	120.00	[35]
0.00	0.00	–	0.20	–	–	0.00	20.00	70.00	–	–	–	–	10.00	–	–	23.00	28.00	145.00	[35]
0.00	0.00	–	0.30	–	–	0.00	20.00	70.00	–	–	–	–	10.00	–	–	23.00	28.00	121.00	[14]

Table 7 (continued)

l/d	SF_V	W (kg)	W/B	S/B	F (mm)	FA (kg)	SF (kg)	GGBS (kg)	SH (kg)	SS (kg)	SS/SH	M	QP (kg)	QS (kg)	SM (kg)	C_T (°C)	C_D (Days)	FC ((MPa)	Refs.
0.00	0.00	–	0.30	–	–	0.00	20.00	70.00	–	–	–	–	10.00	–	–	23.00	90.00	144.00	[14]
0.00	0.00	–	0.30	–	–	0.00	20.00	70.00	–	–	–	–	10.00	–	–	23.00	90.00	130.00	[14]
0.00	0.00	–	0.20	–	–	0.00	20.00	70.00	–	–	–	–	10.00	–	–	23.00	90.00	165.00	[14]
0.00	0.00	–	0.30	–	–	0.00	20.00	70.00	–	–	–	–	10.00	–	–	23.00	90.00	145.00	[14]
0.00	0.00	–	0.30	–	–	–	5.00	–	–	–	–	–	8.00	50.00	–	20.00	28.00	149.80	[14]
0.00	0.00	–	0.30	–	–	–	10.00	–	–	–	–	–	8.00	50.00	–	20.00	28.00	168.30	[14]
0.00	0.00	–	0.30	–	–	–	15.00	–	–	–	–	–	8.00	50.00	–	20.00	28.00	178.60	[14]
0.00	0.00	–	0.30	–	–	–	20.00	–	–	–	–	–	8.00	50.00	–	20.00	28.00	157.50	[14]
0.00	0.00	–	0.30	–	–	–	5.00	–	–	–	–	–	8.00	50.00	–	20.00	28.00	163.80	[14]
0.00	0.00	–	0.30	–	–	–	10.00	–	–	–	–	–	8.00	50.00	–	20.00	28.00	165.00	[14]
0.00	0.00	–	0.30	–	–	–	15.00	–	–	–	–	–	8.00	50.00	–	20.00	28.00	157.00	[14]
0.00	0.00	–	0.30	–	–	–	20.00	–	–	–	–	–	8.00	50.00	–	20.00	28.00	141.60	[14]
0.00	0.00	211.60	0.30	–	163.50	–	12.00	31.50	-	74.90	–	–	7.60	74.20	–	20.00	28.00	123.10	[36]
0.00	0.00	207.60	0.30	–	172.50	–	17.70	27.00	-	101.20	–	–	7.50	72.80	–	20.00	28.00	128.50	[36]
0.00	0.00	–	0.30	–	197.80	–	9.40	90.60	–	–	–	–	–	–	–	30.00	3.00	80.10	[16]
0.00	0.00	–	0.30	–	197.80	–	9.40	90.60	–	-	–	–	–	–	–	30.00	7.00	106.50	[16]
0.00	0.00	–	0.30	–	197.80	–	9.40	90.60	–	-	–	–	–	–	–	30.00	28.00	121.30	[16]
0.00	0.00	–	0.30	–	–	–	13.80	24.80	–	175.00	–	–	7.40	46.00	–	20.00	7.00	108.00	[37]
0.00	0.00	–	0.20	–	–	–	13.80	24.80	–	0.00	–	–	7.30	45.80	–	20.00	7.00	162.90	[37]
0.00	0.00	–	0.20	–	–	–	14.60	26.30	–	0.00	–	–	7.80	48.60	–	20.00	7.00	188.40	[37]
0.00	0.00	114.00	0.30	–	–	–	2.90	35.40	–	0.00	–	–	7.30	45.50	–	20.00	7.00	124.90	[37]
0.00	0.00	–	0.30	–	–	–	13.80	24.80	–	175.00	–	–	7.40	46.00	–	20.00	28.00	157.50	37]
0.00	0.00	–	0.20	–	–	–	13.80	24.80	–	0.00	–	–	7.30	45.80	–	20.00	28.00	194.20	[37]
0.00	0.00	–	0.20	–	–	–	14.60	26.30	–	0.00	–	–	7.80	48.60	–	20.00	28.00	211.80	[37]
0.00	0.00	114.00	0.30	–	–	–	2.90	35.40	–	0.00	–	–	7.30	45.50	–	20.00	28.00	155.30	[37]
0.00	0.00	–	0.30	–	–	–	15.00	–	–	–	–	–	8.00	50.00	–	20.00	7.00	108.00	[38]
0.00	0.00	–	0.20	–	–	–	15.00	–	–	–	–	–	8.00	50.00	–	20.00	7.00	162.90	[38]
0.00	0.00	–	0.20	–	–	–	15.00	–	–	–	–	–	8.00	50.00	–	20.00	7.00	188.40	[38]
0.00	0.00	–	0.20	–	–	–	-	–	–	–	–	–	8.00	50.00	–	20.00	7.00	190.90	[38]
0.00	0.00	–	0.30	–	–	–	15.00	–	–	–	–	–	8.00	50.00	–	20.00	28.00	157.50	[38]
0.00	0.00	–	0.20	–	–	–	15.00	–	–	–	–	–	8.00	50.00	–	20.00	28.00	194.20	[38]
0.00	0.00	–	0.20	–	–	–	15.00	–	–	–	–	–	8.00	50.00	–	20.00	28.00	211.80	[38]
0.00	0.00	–	0.20	–	–	–	–	–	–	–	–	–	8.00	50.00	–	20.00	28.00	212.80	[38]
0.00	0.00	230.00	–	–	–	–	10.00	90.00	–	–	–	–	–	–	9.50	60.00	3.00	151.10	[39]
0.00	0.00	230.00	–	–	–	–	10.00	80.00	–	–	–	–	–	–	9.50	60.00	3.00	133.30	[39]
0.00	0.00	230.00	–	–	–	–	10.00	60.00	–	–	–	–	–	–	9.50	60.00	3.00	140.50	[39]

Table 7 (continued)

l/d	SF_V	W (kg)	W/B	S/B	F (mm)	FA (kg)	SF (kg)	GGBS (kg)	SH (kg)	SS (kg)	SS/SH	M	QP (kg)	QS (kg)	SM (kg)	C_T (°C)	C_D (Days)	FC ((MPa)	Refs.
0.00	0.00	230.00	–	–	–	–	10.00	40.00	–	–	–	–	–	–	9.50	60.00	3.00	134.50	[39]
0.00	0.00	230.00	–	–	–	–	10.00	20.00	–	–	–	–	–	–	9.50	60.00	3.00	115.10	[39]
0.00	0.00	230.00	–	–	–	–	10.00	90.00	–	–	–	–	–	–	9.50	60.00	7.00	142.60	[39]
0.00	0.00	230.00	–	–	–	–	10.00	80.00	–	–	–	–	–	–	9.50	60.00	7.00	146.00	[39]
0.00	0.00	230.00	–	–	–	–	10.00	60.00	–	–	–	–	–	–	9.50	60.00	7.00	155.30	[39]
0.00	0.00	230.00	–	–	–	–	10.00	40.00	–	–	–	–	–	–	9.50	60.00	7.00	145.10	[39]
0.00	0.00	230.00	–	–	–	–	10.00	20.00	–	–	–	–	–	–	9.50	60.00	7.00	135.10	[39]
0.00	0.00	230.00	–	–	–	–	10.00	90.00	–	–	–	–	–	–	9.50	60.00	28.00	135.90	[39]
0.00	0.00	230.00	–	–	–	–	10.00	80.00	–	–	–	–	–	–	9.50	60.00	28.00	141.90	[39]
0.00	0.00	230.00	–	–	–	–	10.00	60.00	–	–	–	–	–	–	9.50	60.00	28.00	156.10	[39]
0.00	0.00	230.00	–	–	–	–	10.00	40.00	–	–	–	–	–	–	9.50	60.00	28.00	149.70	[39]
0.00	0.00	230.00	–	–	–	–	10.00	20.00	–	–	–	–	–	–	9.50	60.00	28.00	138.40	[39]
108.30	3.00	–	0.40	–	–	–	8.30	74.90	–	16.80	–	–	–	–	–	25.00	28.00	123.00	[40]
108.30	3.00	–	0.40	–	–	–	16.70	66.50	–	16.80	–	–	–	–	–	25.00	28.00	133.30	[40]
108.30	0.00	–	0.40	–	–	–	20.70	64.50	–	16.80	–	–	–	–	–	25.00	7.00	80.00	[40]
108.30	0.00	–	0.40	–	–	–	20.70	64.50	–	16.80	–	–	–	–	–	25.00	14.00	110.00	[40]
108.30	0.00	–	0.40	–	–	–	20.70	64.50	–	16.80	–	–	–	–	–	25.00	90.00	128.00	[40]
108.30	1.00	–	0.40	–	–	–	20.70	64.50	–	16.80	–	–	–	–	–	25.00	28.00	127.00	[40]
108.30	2.00	–	0.40	–	–	–	20.70	64.50	–	16.80	–	–	–	–	–	25.00	28.00	139.00	[40]
108.30	3.00	–	0.40	–	–	–	20.70	64.50	–	16.80	–	–	–	–	–	25.00	7.00	100.00	[40]
108.30	3.00	–	0.40	–	–	–	20.70	64.50	–	16.80	–	–	–	–	–	25.00	14.00	132.00	[40]
108.30	3.00	–	0.40	–	–	–	20.70	64.50	–	16.80	–	–	–	–	–	25.00	90.00	165.00	[40]
65.00	3.00	–	0.20	–	–	44.80	6.30	29.90	–	11.40	–	–	–	–	7.70	25.00	1.00	163.00	[41]
65.00	3.00	–	0.20	–	–	29.90	6.30	44.80	–	11.40	–	–	–	–	7.70	25.00	1.00	191.00	[41]
65.00	3.00	–	0.20	–	–	14.90	6.30	59.70	–	11.40	–	–	–	–	7.70	25.00	1.00	210.00	[41]
65.00	2.00	–	0.20	–	–	14.90	6.30	59.70	–	11.40	–	–	–	–	7.70	25.00	1.00	199.00	[41]
65.00	4.00	–	0.20	–	–	14.90	6.30	59.70	–	11.40	–	–	–	–	7.70	25.00	1.00	222.00	[41]
125.00	2.00	88.00	0.30	–	–	13.00	52.70	–	3.50	24.10	6.90	–	–	–	–	25.00	28.00	130.00	[42]
125.00	3.00	88.00	0.30	–	–	13.00	52.70	–	3.50	24.10	6.90	–	–	–	–	25.00	28.00	150.00	[42]
0.00	0.00	–	0.30	–	324.00	8.40	5.20	52.50	3.90	30.00	7.70	–	–	–	–	23.00	3.00	134.90	[43]
0.00	0.00	–	0.30	–	332.00	8.40	5.20	189.60	11.20	86.70	7.70	–	–	–	–	23.00	3.00	150.50	[43]
0.00	0.00	–	0.30	–	342.00	8.40	5.20	37.00	3.10	23.60	7.50	–	–	–	–	23.00	3.00	129.80	[43]
0.00	0.00	–	0.30	–	354.00	8.40	5.20	13.00	1.80	13.70	7.70	–	–	–	–	23.00	3.00	118.70	[43]
0.00	0.00	–	0.30	–	321.00	113.10	5.20	52.50	9.50	73.30	7.70	–	–	–	–	23.00	3.00	120.40	[43]
0.00	0.00	–	0.30	–	300.00	55.40	5.20	52.50	6.40	49.40	7.70	–	–	–	–	23.00	3.00	145.60	[43]
0.00	0.00	–	0.30	–	285.00	26.00	5.20	52.50	4.80	37.30	7.70	–	–	–	–	23.00	3.00	140.80	[43]

Table 7 (continued)

l/d	SF_V	W (kg)	W/B	S/B	F (mm)	FA (kg)	SF (kg)	GGBS (kg)	SH (kg)	SS (kg)	SS/SH	M	QP (kg)	QS (kg)	SM (kg)	C_T (°C)	C_D (Days)	FC ((MPa)	Refs.
0.00	0.00	–	0.30	–	324.00	8.40	5.20	52.50	3.90	30.00	7.70	–	–	–	–	23.00	7.00	138.30	[43]
0.00	0.00	–	0.30	–	332.00	8.40	5.20	189.60	11.20	86.70	7.70	–	–	–	–	23.00	7.00	155.10	[43]
0.00	0.00	–	0.30	–	342.00	8.40	5.20	37.00	3.10	23.60	7.50	–	–	–	–	23.00	7.00	134.50	[43]
0.00	0.00	–	0.30	–	354.00	8.40	5.20	13.00	1.80	13.70	7.70	–	–	–	–	23.00	7.00	121.00	[43]
0.00	0.00	–	0.30	–	321.00	113.10	5.20	52.50	9.50	73.30	7.70	–	–	–	–	23.00	7.00	125.60	[43]
0.00	0.00	–	0.30	–	300.00	55.40	5.20	52.50	6.40	49.40	7.70	–	–	–	–	23.00	7.00	150.30	[43]
0.00	0.00	–	0.30	–	285.00	26.00	5.20	52.50	4.80	37.30	7.70	–	–	–	–	23.00	7.00	145.60	[43]
0.00	0.00	–	0.30	–	324.00	8.40	5.20	52.50	3.90	30.00	7.70	–	–	–	–	23.00	28.00	140.30	[43]
0.00	0.00	–	0.30	–	332.00	8.40	5.20	189.60	11.20	86.70	7.70	–	–	–	–	23.00	28.00	159.60	[43]
0.00	0.00	–	0.30	–	342.00	8.40	5.20	37.00	3.10	23.60	7.50	–	–	–	–	23.00	28.00	137.60	[43]
0.00	0.00	–	0.30	–	354.00	8.40	5.20	13.00	1.80	13.70	7.70	–	–	–	–	23.00	28.00	127.50	[43]
0.00	0.00	–	0.30	–	321.00	113.10	5.20	52.50	9.50	73.30	7.70	–	–	–	–	23.00	28.00	129.50	[43]
0.00	0.00	–	0.30	–	300.00	55.40	5.20	52.50	6.40	49.40	7.70	–	–	–	–	23.00	28.00	153.20	[43]
0.00	0.00	–	0.30	–	285.00	26.00	5.20	52.50	4.80	37.30	7.70	–	–	–	–	23.00	28.00	149.60	[43]
65.00	0.80	–	–	–	–	–	12.00	36.00	4.20	12.60	3.00	16.00	–	35.90	–	25.00	7.00	109.40	[44]
65.00	1.30	–	–	–	–	–	12.00	36.00	4.20	12.60	3.00	16.00	–	35.90	–	25.00	7.00	114.80	[44]
65.00	1.80	–	–	–	–	–	12.00	36.00	4.20	12.60	3.00	16.00	–	35.90	–	25.00	7.00	117.80	[44]
65.00	1.00	–	–	–	–	–	12.00	36.00	4.20	12.60	3.00	16.00	–	35.90	–	25.00	7.00	112.90	[44]
65.00	1.50	–	–	–	–	–	12.00	36.00	4.20	12.60	3.00	16.00	–	35.90	–	25.00	7.00	116.30	[44]
65.00	2.00	–	–	–	–	–	12.00	36.00	4.20	12.60	3.00	16.00	–	35.90	–	25.00	7.00	121.00	[44]
65.00	0.80	–	–	–	–	–	12.00	36.00	4.20	12.60	3.00	16.00	–	35.90	–	25.00	28.00	134.00	[44]
65.00	1.30	–	–	–	–	–	12.00	36.00	4.20	12.60	3.00	16.00	–	35.90	–	25.00	28.00	139.60	[44]
65.00	1.80	–	–	–	–	–	12.00	36.00	4.20	12.60	3.00	16.00	–	35.90	–	25.00	28.00	145.30	[44]
65.00	1.00	–	–	–	–	–	12.00	36.00	4.20	12.60	3.00	16.00	–	35.90	–	25.00	28.00	138.00	[44]
65.00	1.50	–	–	–	–	–	12.00	36.00	4.20	12.60	3.00	16.00	–	35.90	–	25.00	28.00	142.10	[44]
65.00	2.00	–	–	–	–	–	12.00	36.00	4.20	12.60	3.00	16.00	–	35.90	–	25.00	28.00	150.60	[44]
65.00	0.80	–	–	–	–	–	12.00	36.00	4.20	12.60	3.00	16.00	–	35.90	–	25.00	90.00	147.80	[44]
65.00	1.30	–	–	–	–	–	12.00	36.00	4.20	12.60	3.00	16.00	–	35.90	–	25.00	90.00	154.70	[44]
65.00	1.80	–	–	–	–	–	12.00	36.00	4.20	12.60	3.00	16.00	–	35.90	–	25.00	90.00	161.60	[44]
65.00	1.00	–	–	–	–	–	12.00	36.00	4.20	12.60	3.00	16.00	–	35.90	–	25.00	90.00	150.70	[44]
65.00	1.50	–	–	–	–	–	12.00	36.00	4.20	12.60	3.00	16.00	–	35.90	–	25.00	90.00	158.40	[44]
65.00	2.00	–	–	–	–	–	12.00	36.00	4.20	12.60	3.00	16.00	–	35.90	–	25.00	90.00	168.00	[44]
125.00	1.00	–	–	–	–	–	–	48.50	14.00	–	–	–	–	47.90	2.80	25.00	7.00	115.00	[45]
125.00	1.30	–	–	–	–	–	–	48.50	14.00	–	–	–	–	47.90	2.80	25.00	7.00	123.00	[45]
125.00	1.50	–	–	–	–	–	–	48.50	14.00	–	–	–	–	47.90	2.80	25.00	7.00	127.00	[45]
125.00	1.80	–	–	–	–	–	–	48.50	14.00	–	–	–	–	47.90	2.80	25.00	7.00	122.00	[45]

Table 7 (continued)

l/d	SF_V	W (kg)	W/B	S/B	F (mm)	FA (kg)	SF (kg)	GGBS (kg)	SH (kg)	SS (kg)	SS/SH	M	QP (kg)	QS (kg)	SM (kg)	C_T (°C)	C_D (Days)	FC ((MPa)	Refs.
125.00	2.00	–	–	–	–	–	–	48.50	14.00	–	–	–	–	47.90	2.80	25.00	7.00	126.00	[45]
125.00	2.30	–	–	–	–	–	–	48.50	14.00	–	–	–	–	47.90	2.80	25.00	7.00	129.00	[45]
125.00	1.00	–	–	–	–	–	–	48.50	14.00	–	–	–	–	47.90	2.80	25.00	28.00	140.00	[45]
125.00	1.30	–	–	–	–	–	–	48.50	14.00	–	–	–	–	47.90	2.80	25.00	28.00	144.00	[45]
125.00	1.50	–	–	–	–	–	–	48.50	14.00	–	–	–	–	47.90	2.80	25.00	28.00	150.00	[45]
125.00	1.80	–	–	–	–	–	–	48.50	14.00	–	–	–	–	47.90	2.80	25.00	28.00	147.00	[45]
125.00	2.00	–	–	–	–	–	–	48.50	14.00	–	–	–	–	47.90	2.80	25.00	28.00	152.00	[45]
125.00	2.30	–	–	–	–	–	–	48.50	14.00	–	–	–	–	47.90	2.80	25.00	28.00	162.00	[45]
125.00	1.00	–	–	–	–	–	–	48.50	14.00	–	–	–	–	47.90	2.80	25.00	90.00	149.00	[45]
125.00	1.30	–	–	–	–	–	–	48.50	14.00	–	–	–	–	47.90	2.80	25.00	90.00	157.00	[45]
125.00	1.50	–	–	–	–	–	–	48.50	14.00	–	–	–	–	47.90	2.80	25.00	90.00	165.00	[45]
125.00	1.80	–	–	–	–	–	–	48.50	14.00	–	–	–	–	47.90	2.80	25.00	90.00	159.00	[45]
125.00	2.00	–	–	–	–	–	–	48.50	14.00	–	–	–	–	47.90	2.80	25.00	90.00	158.00	[45]
125.00	2.30	–	–	–	–	–	–	48.50	14.00	–	–	–	–	47.90	2.80	25.00	90.00	175.00	[45]
50.00	0.00	97.00	0.30	1.00	260.00	12.60	3.30	50.60	3.30	23.10	7.00	–	–	–	–	80.00	1.00	103.00	[46]
50.00	1.00	97.00	0.30	1.00	252.00	12.60	3.30	50.60	3.30	23.10	7.00	–	–	–	–	80.00	1.00	140.00	[46]
50.00	2.00	97.00	0.30	1.00	248.00	12.60	3.30	50.60	3.30	23.10	7.00	–	–	–	–	80.00	1.00	158.00	[46]
50.00	3.00	97.00	0.30	1.00	243.00	12.60	3.30	50.60	3.30	23.10	7.00	–	–	–	–	80.00	1.00	170.00	[46]
66.70	1.00	97.00	0.30	1.00	250.10	12.60	3.30	50.60	3.30	23.10	7.00	–	–	–	–	80.00	1.00	133.00	[46]
66.70	2.00	97.00	0.30	1.00	245.00	12.60	3.30	50.60	3.30	23.10	7.00	–	–	–	–	80.00	1.00	146.00	[46]
66.70	3.00	97.00	0.30	1.00	229.00	12.60	3.30	50.60	3.30	23.10	7.00	–	–	–	–	80.00	1.00	160.00	[46]
108.30	1.00	97.00	0.30	1.00	255.10	12.60	3.30	50.60	3.30	23.10	7.00	–	–	–	–	80.00	1.00	138.00	[46]
108.30	2.00	97.00	0.30	1.00	247.10	12.60	3.30	50.60	3.30	23.10	7.00	–	–	–	–	80.00	1.00	148.00	[46]
108.30	3.00	97.00	0.30	1.00	230.00	12.60	3.30	50.60	3.30	23.10	7.00	–	–	–	–	80.00	1.00	166.00	[46]
65.00	1.00	97.00	0.30	1.00	255.20	12.60	3.30	50.60	3.30	23.10	7.00	–	–	–	–	80.00	1.00	126.00	[46]
65.00	2.00	97.00	0.30	1.00	247.00	12.60	3.30	50.60	3.30	23.10	7.00	–	–	–	–	80.00	1.00	142.00	[46]
65.00	3.00	97.00	0.30	1.00	240.10	12.60	3.30	50.60	3.30	23.10	7.00	–	–	–	–	80.00	1.00	148.00	[46]
50.00	1.00	97.00	0.30	1.00	252.00	12.60	3.30	50.60	3.30	23.10	7.00	–	–	–	–	20.00	28.00	142.00	[46]
50.00	2.00	97.00	0.30	1.00	248.00	12.60	3.30	50.60	3.30	23.10	7.00	–	–	–	–	20.00	28.00	150.00	[46]
50.00	3.00	97.00	0.30	1.00	243.00	12.60	3.30	50.60	3.30	23.10	7.00	–	–	–	–	20.00	28.00	155.00	[46]
66.70	1.00	97.00	0.30	1.00	250.10	12.60	3.30	50.60	3.30	23.10	7.00	–	–	–	–	20.00	28.00	142.00	[46]
66.70	2.00	97.00	0.30	1.00	245.00	12.60	3.30	50.60	3.30	23.10	7.00	–	–	–	–	20.00	28.00	158.00	[46]
66.70	3.00	97.00	0.30	1.00	229.00	12.60	3.30	50.60	3.30	23.10	7.00	–	–	–	–	20.00	28.00	168.00	[46]
108.30	1.00	97.00	0.30	1.00	255.10	12.60	3.30	50.60	3.30	23.10	7.00	–	–	–	–	20.00	28.00	144.00	[46]
108.30	2.00	97.00	0.30	1.00	247.10	12.60	3.30	50.60	3.30	23.10	7.00	–	–	–	–	20.00	28.00	162.00	[46]
108.30	3.00	97.00	0.30	1.00	230.00	12.60	3.30	50.60	3.30	23.10	7.00	–	–	–	–	20.00	28.00	171.00	[46]

Table 7 (continued)

l/d	SF_V	W (kg)	W/B	S/B	F (mm)	FA (kg)	SF (kg)	GGBS (kg)	SH (kg)	SS (kg)	SS/SH	M	QP (kg)	QS (kg)	SM (kg)	C_T (°C)	C_D (Days)	FC ((MPa)	Refs.
65.00	1.00	97.00	0.30	1.00	255.20	12.60	3.30	50.60	3.30	23.10	7.00	–	–	–	–	20.00	28.00	132.00	[46]
65.00	2.00	97.00	0.30	1.00	247.00	12.60	3.30	50.60	3.30	23.10	7.00	–	–	–	–	20.00	28.00	141.00	[46]
65.00	3.00	97.00	0.30	1.00	240.10	12.60	3.30	50.60	3.30	23.10	7.00	–	–	–	–	20.00	28.00	151.00	[46]
37.50	1.00	8.40	0.40	–	130.00	0.00	24.00	76.00	–	7.60	–	–	–	–	–	23.00	1.00	60.00	[47]
0.00	0.00	8.40	0.40	–	105.00	33.00	24.00	43.00	–	7.60	–	–	–	–	–	23.00	1.00	33.40	[47]
37.50	1.00	8.40	0.40	–	105.00	33.00	24.00	43.00	–	7.60	–	–	–	–	–	23.00	1.00	35.60	[47]
37.50	1.00	8.40	0.40	–	125.00	0.00	24.00	76.00	–	–	–	–	–	–	–	23.00	1.00	59.00	[47]
0.00	0.00	8.40	0.40	–	132.00	0.00	24.00	76.00	–	–	–	–	–	–	–	23.00	1.00	59.00	[47]
81.30	1.00	8.40	0.40	–	113.00	0.00	24.00	76.00	–	–	–	–	–	–	–	23.00	1.00	60.00	[47]
81.30	2.00	8.40	0.40	–	103.00	0.00	24.00	76.00	–	–	–	–	–	–	–	23.00	1.00	66.00	[47]
81.30	2.00	8.40	0.40	–	107.00	0.00	24.00	76.00	–	–	–	–	–	–	–	23.00	1.00	62.00	[47]
37.50	1.00	8.40	0.40	–	125.00	0.00	24.00	76.00	–	–	–	–	–	–	–	23.00	7.00	97.00	[47]
0.00	0.00	8.40	0.40	–	132.00	0.00	24.00	76.00	–	–	–	–	–	–	–	23.00	7.00	87.00	[47]
81.30	1.00	8.40	0.40	–	113.00	0.00	24.00	76.00	–	–	–	–	–	–	–	23.00	7.00	101.00	[47]
81.30	2.00	8.40	0.40	–	103.00	0.00	24.00	76.00	–	–	–	–	–	–	–	23.00	7.00	125.00	[47]
81.30	2.00	8.40	0.40	–	107.00	0.00	24.00	76.00	–	–	–	–	–	–	–	23.00	7.00	116.00	[47]
37.50	1.00	8.40	0.40	–	130.00	0.00	24.00	76.00	–	7.60	–	–	–	–	–	23.00	14.00	120.00	[47]
37.50	1.00	8.40	0.40	–	125.00	0.00	24.00	76.00	–	–	–	–	–	–	–	23.00	14.00	124.00	[47]
0.00	0.00	8.40	0.40	–	132.00	0.00	24.00	76.00	–	–	–	–	–	–	–	23.00	14.00	118.00	[47]
81.30	1.00	8.40	0.40	–	113.00	0.00	24.00	76.00	–	–	–	–	–	–	–	23.00	14.00	140.00	[47]
81.30	2.00	8.40	0.40	–	103.00	0.00	24.00	76.00	–	–	–	–	–	–	–	23.00	14.00	160.00	[47]
81.30	2.00	8.40	0.40	–	107.00	0.00	24.00	76.00	–	–	–	–	–	–	–	23.00	14.00	148.00	[47]
37.50	1.00	8.40	0.40	–	130.00	0.00	24.00	76.00	–	7.60	–	–	–	–	–	23.00	28.00	122.00	[47]
37.50	1.00	8.40	0.40	–	125.00	0.00	24.00	76.00	–	–	–	–	–	–	–	23.00	28.00	130.00	[47]
0.00	0.00	8.40	0.40	–	132.00	0.00	24.00	76.00	–	–	–	–	–	–	–	23.00	28.00	124.00	[47]
81.30	1.00	8.40	0.40	–	113.00	0.00	24.00	76.00	–	–	–	–	–	–	–	23.00	28.00	144.00	[47]
81.30	2.00	8.40	0.40	–	103.00	0.00	24.00	76.00	–	–	–	–	–	–	–	23.00	28.00	175.00	[47]
81.30	2.00	8.40	0.40	–	107.00	0.00	24.00	76.00	–	–	–	–	–	–	–	23.00	28.00	154.00	[47]
65.00	2.00	260.00	0.30	–	–	13.20	5.50	52.70	–	10.10	–	–	–	–	–	23.00	7.00	135.80	[48]
65.00	2.00	260.00	0.30	–	–	13.20	5.50	52.70	–	10.10	–	–	–	–	3.40	23.00	7.00	186.00	[48]
65.00	2.00	260.00	0.30	–	–	13.20	5.50	52.70	–	10.10	–	–	–	–	6.80	23.00	7.00	179.00	[48]
61.90	1.00	250.00	0.30	–	–	5.90	2.00	31.40	2.90	–	–	–	39.20	–	8.80	23.00	28.00	140.00	[49]
61.90	2.00	250.00	0.30	–	–	5.90	2.00	31.40	2.90	–	–	–	39.20	–	8.80	23.00	28.00	150.00	[49]
66.70	2.00	–	0.30	–	–	–	9.00	51.20	7.20	10.80	1.50	1.50	21.70	–	–	29.00	7.00	79.00	[50]
66.70	1.00	–	0.30	–	–	–	8.40	47.80	6.70	10.10	1.50	1.50	27.00	–	–	29.00	7.00	80.00	[50]
66.70	2.00	–	0.30	–	–	–	8.40	47.80	6.70	10.10	1.50	1.50	27.00	–	–	29.00	7.00	95.00	[50]

Table 7 (continued)

l/d	SF_V	W (kg)	W/B	S/B	F (mm)	FA (kg)	SF (kg)	GGBS (kg)	SH (kg)	SS (kg)	SS/SH	M	QP (kg)	QS (kg)	SM (kg)	C_T (°C)	C_D (Days)	FC ((MPa)	Refs.
66.70	2.00	–	0.30	–	–	–	19.50	45.50	7.80	11.70	1.50	1.50	15.60	–	–	29.00	7.00	76.00	[50]
66.70	1.00	–	0.30	–	–	–	18.10	42.20	7.20	10.80	1.50	1.50	21.70	–	–	29.00	7.00	82.00	[50]
66.70	2.00	–	0.30	–	–	–	18.10	42.20	7.20	10.80	1.50	1.50	21.70	–	–	29.00	7.00	87.00	[50]
66.70	0.00	–	0.30	–	–	–	16.90	39.30	6.70	10.10	1.50	1.50	27.00	–	–	29.00	7.00	80.00	[50]
66.70	1.00	–	0.30	–	–	–	16.90	39.30	6.70	10.10	1.50	1.50	27.00	–	–	29.00	7.00	95.00	[50]
66.70	2.00	–	0.30	–	–	–	16.90	39.30	6.70	10.10	1.50	1.50	27.00	–	–	29.00	7.00	106.00	[50]
66.70	2.00	–	0.30	–	–	–	9.00	51.20	7.20	10.80	1.50	1.50	21.70	–	–	29.00	28.00	121.00	[50]
66.70	1.00	–	0.30	–	–	–	8.40	47.80	6.70	10.10	1.50	1.50	27.00	–	–	29.00	28.00	120.00	[50]
66.70	2.00	–	0.30	–	–	–	8.40	47.80	6.70	10.10	1.50	1.50	27.00	–	–	29.00	28.00	130.00	[50]
66.70	2.00	–	0.30	–	–	–	19.50	45.50	7.80	11.70	1.50	1.50	15.60	–	–	29.00	28.00	123.00	[50]
66.70	1.00	–	0.30	–	–	–	18.10	42.20	7.20	10.80	1.50	1.50	21.70	–	–	29.00	28.00	120.00	[50]
66.70	2.00	–	0.30	–	–	–	18.10	42.20	7.20	10.80	1.50	1.50	21.70	–	–	29.00	28.00	130.00	[50]
66.70	0.00	–	0.30	–	–	–	16.90	39.30	6.70	10.10	1.50	1.50	27.00	–	–	29.00	28.00	120.00	[50]
66.70	1.00	–	0.30	–	–	–	16.90	39.30	6.70	10.10	1.50	1.50	27.00	–	–	29.00	28.00	135.00	[50]
66.70	2.00	–	0.30	–	–	–	16.90	39.30	6.70	10.10	1.50	1.50	27.00	–	–	29.00	28.00	148.00	[50]
0.00	0.00	–	0.20	–	–	–	11.80	35.40	10.60	31.80	3.00	8.00	–	39.40	–	25.00	3.00	113.00	[51]
0.00	0.00	–	0.20	–	–	–	11.80	35.40	10.60	31.80	3.00	8.00	–	39.40	–	25.00	7.00	118.00	[51]
0.00	0.00	–	1.50	–	–	–	11.80	35.40	10.60	31.80	3.00	12.00	–	39.40	–	25.00	28.00	122.00	[51]
0.00	0.00	–	0.10	–	–	–	11.80	35.40	10.60	31.80	3.00	16.00	–	39.40	–	25.00	28.00	130.00	[51]
65.00	1.00	–	0.40	–	–	–	11.80	35.40	4.10	12.40	3.00	16.00	–	35.20	–	25.00	28.00	138.00	[51]
65.00	1.50	–	0.40	–	–	–	11.80	35.40	4.10	12.40	3.00	16.00	–	35.20	–	25.00	28.00	142.10	[51]
65.00	2.00	–	0.40	–	–	–	11.80	35.40	4.10	12.40	3.00	16.00	–	35.20	–	25.00	28.00	150.60	[51]
0.00	0.00	–	–	–	–	–	10.40	62.40	-	27.20	-	4.00	–	–	–	20.00	1.00	63.10	[52]
70.00	1.00	–	–	–	–	–	10.40	62.40	-	27.20	-	4.00	–	–	–	20.00	1.00	93.40	[52]
70.00	2.00	–	–	–	–	–	10.40	62.40	-	27.20	-	4.00	–	–	–	20.00	1.00	99.80	[52]
0.00	0.00	–	–	–	–	–	10.40	62.40	-	27.20	-	8.00	–	–	–	20.00	1.00	72.30	[52]
70.00	1.00	–	–	–	–	–	10.40	62.40	-	27.20	-	8.00	–	–	–	20.00	1.00	105.90	[52]
70.00	2.00	–	–	–	–	–	10.40	62.40	-	27.20	-	8.00	–	–	–	20.00	1.00	125.60	[52]
0.00	0.00	–	–	–	–	–	10.40	62.40	-	27.20	-	12.00	–	–	–	20.00	1.00	96.10	[52]
70.00	1.00	–	–	–	–	–	10.40	62.40	-	27.20	-	12.00	–	–	–	20.00	1.00	130.60	[52]
70.00	2.00	–	–	–	–	–	10.40	62.40	-	27.20	-	12.00	–	–	–	20.00	1.00	136.30	[52]
97.50	2.00	396.00	0.30	0.20	–	–	8.80	58.80	3.20	9.50	3.00	–	–	–	–	20.00	1.00	139.00	[17]
97.50	2.00	349.00	0.30	0.30	–	–	8.00	53.10	2.80	8.40	3.00	–	–	–	–	20.00	1.00	142.00	[17]
97.50	2.00	315.00	0.30	0.50	–	–	7.30	48.60	2.50	7.60	3.00	–	–	–	–	20.00	1.00	145.00	[17]
97.50	2.00	291.00	0.30	0.60	–	–	6.70	44.80	2.40	7.00	3.00	–	–	–	–	20.00	1.00	146.90	[17]
97.50	2.00	270.00	0.30	0.80	–	–	6.30	41.60	2.20	6.50	3.00	–	–	–	–	20.00	1.00	160.70	[17]

Table 7 (continued)

l/d	SF_V	W (kg)	W/B	S/B	F (mm)	FA (kg)	SF (kg)	GGBS (kg)	SH (kg)	SS (kg)	SS/SH	M	QP (kg)	QS (kg)	SM (kg)	C_T (°C)	C_D (Days)	FC ((MPa)	Refs.
0.00	–	396.00	0.30	0.20	–	–	8.80	58.80	3.20	9.50	3.00	–	–	–	–	20.00	1.00	131.00	[19]
0.00	–	349.00	0.30	0.30	–	–	8.00	53.10	2.80	8.40	3.00	–	–	–	–	20.00	1.00	125.00	[19]
0.00	–	315.00	0.30	0.50	–	–	7.30	48.60	2.50	7.60	3.00	–	–	–	–	20.00	1.00	130.00	[19]
0.00	–	291.00	0.30	0.60	–	–	6.70	44.80	2.40	7.00	3.00	–	–	–	–	20.00	1.00	135.00	[19]
97.50	2.00	396.00	0.30	0.20	–	–	8.80	58.80	3.20	9.50	3.00	–	–	–	–	20.00	1.00	146.00	[19]
97.50	2.00	349.00	0.30	0.30	–	–	8.00	53.10	2.80	8.40	3.00	–	–	–	–	20.00	1.00	147.00	[19]
97.50	2.00	315.00	0.30	0.50	–	–	7.30	48.60	2.50	7.60	3.00	–	–	–	–	20.00	1.00	150.00	[19]
97.50	2.00	291.00	0.30	0.60	–	–	6.70	44.80	2.40	7.00	3.00	–	–	–	–	20.00	1.00	159.00	[19]
37.50	0.00	49.00	0.20	–	–	–	7.70	30.80	1.30	6.80	5.20	–	–	53.30	–	20.00	1.00	132.00	[53]
37.50	0.50	49.00	0.20	–	–	–	7.70	30.80	1.30	6.80	5.20	–	–	53.30	–	20.00	1.00	172.00	[53]
37.50	1.00	49.00	0.20	–	–	–	7.70	30.80	1.30	6.80	5.20	–	–	53.30	–	20.00	1.00	181.00	[53]
37.50	1.50	49.00	0.20	–	–	–	7.70	30.80	1.30	6.80	5.20	–	–	53.30	–	20.00	1.00	192.00	[53]
37.50	2.00	49.00	0.20	–	–	–	7.70	30.80	1.30	6.80	5.20	–	–	53.30	–	20.00	1.00	195.00	[53]
81.30	0.00	49.00	0.20	–	–	–	7.70	30.80	1.30	6.80	5.20	–	–	53.30	–	20.00	1.00	132.00	[53]
81.30	0.50	49.00	0.20	–	–	–	7.70	30.80	1.30	6.80	5.20	–	–	53.30	–	20.00	1.00	177.00	[53]
81.30	1.00	49.00	0.20	–	–	–	7.70	30.80	1.30	6.80	5.20	–	–	53.30	–	20.00	1.00	193.00	[53]
81.30	1.50	49.00	0.20	–	–	–	7.70	30.80	1.30	6.80	5.20	–	–	53.30	–	20.00	1.00	223.00	[53]
81.30	2.00	49.00	0.20	–	–	172.00	7.70	30.80	1.30	6.80	5.20	–	–	53.30	–	20.00	1.00	229.00	[53]
108.30	0.00	87.00	0.30	1.00	–	172.00	2.30	34.50	2.30	15.70	7.00	–	–	45.30	–	80.00	1.00	101.40	[54]
108.30	1.00	87.00	0.30	1.00	–	172.00	2.30	34.50	2.30	15.70	7.00	–	–	45.30	–	80.00	1.00	108.50	[54]
108.30	2.00	87.00	0.30	1.00	–	172.00	2.30	34.50	2.30	15.70	7.00	–	–	45.30	–	80.00	1.00	127.50	[54]
108.30	3.00	87.00	0.30	1.00	–	163.00	2.30	34.50	2.30	15.70	7.00	–	–	45.30	–	80.00	1.00	154.90	[54]
108.30	2.00	87.00	0.30	1.00	–	145.00	4.50	32.60	2.30	15.70	7.00	–	–	45.30	–	80.00	1.00	104.00	[54]
108.30	2.00	87.00	0.30	1.00	–	127.00	9.00	29.00	2.30	15.70	7.00	–	–	45.30	–	80.00	1.00	137.00	[54]
108.30	2.00	87.00	0.30	1.00	–	–	13.50	25.40	2.30	15.70	7.00	–	–	45.30	–	80.00	1.00	150.00	[54]
0.00	–	–	0.30	–	220.00	–	15.00	27.00	–	–	–	–	8.00	50.00	–	20.00	7.00	108.00	[38]
0.00	–	–	0.20	–	340.00	–	15.00	27.00	–	–	–	–	8.00	50.00	–	20.00	7.00	162.90	[38]
0.00	–	–	0.20	–	300.00	–	15.00	27.00	–	–	–	–	8.00	50.00	–	20.00	7.00	188.40	[38]
0.00	–	–	0.30	–	220.00	–	15.00	27.00	–	–	–	–	8.00	50.00	–	20.00	28.00	157.50	[38]
0.00	–	–	0.20	–	340.00	–	15.00	27.00	–	–	–	–	8.00	50.00	–	20.00	28.00	194.20	[38]
0.00	–	–	0.20	–	300.00	–	15.00	27.00	–	–	–	–	8.00	50.00	–	20.00	28.00	211.80	[38]

curing process, thereby providing crucial insights for real-time decision-making.

The integration of visualization tools within a GUI further enhances its utility. Graphs displaying the compressive strength over curing days provide a clear and intuitive representation of the strength of AA-UHPC. This visual feedback is invaluable for understanding the behavior and performance of a material. In addition, the GUI allows users to predict the strength at any point during the curing period. This flexibility in predicting the strength on-the-fly aids in optimizing curing strategies and allows for timely adjustments, leading to improved concrete quality. Moreover, the GUI significantly reduces computational effort. Developing accurate models to predict compressive strength involves complex calculations, often requiring extensive data analysis and programming using Python software. The GUI combines these computational algorithms into a user-friendly interface, shielding users from intricate details while providing instant results. In addition, it can be used to limit input features; thus, they can be used to compare the results of different values. Furthermore, a GUI fosters a culture of innovation and collaboration. As more engineers and researchers adopt this tool, a shared platform for predicting the AA-UHPC compressive strength can be established. This collective knowledge and data contribute to refining prediction models by improving the GUI database, making them more accurate and representative of a wider range of scenarios. The GUI can also serve as a valuable educational tool, enabling students and novice engineers to explore the behavior of AA-UHPC in a controlled environment.

10 Conclusion

A comprehensive study was performed by applying ML algorithms to determine a surrogate estimation model for estimating compressive strength of AA-UHPC materials, which can facilitate experimental tests and reduce evaluation time and effort. Eighteen input parameters were chosen to construct the ML models, and their influence on the compressive strength at different curing days was investigated. The following conclusions were drawn:

- The flow, followed by the SH, curing duration, water, and molarity, were introduced as the most important features for estimating the compressive strength of AA-UHPC. In addition, flow showed a relative importance about twice as much as morality. In contrast, S/B, SF, SM, and QS were among the variables with the least importance in predicting the target value.
- According to the PDP results, the two features of SF and C_T showed linear behavior, while the features of W, SF_V, M, SS/SH ratio, and C_D showed an increasing trend. By contrast, SH, SS, FA, and W/B exhibited decreasing trends in the estimation of the compressive strength of AA-UHPC. Furthermore, the input features of water, flow, SH, W/B, and C_D had the greatest influence on the target and could not be neglected during the predictions.
- The scatter of actual and predicted values of the compressive strength of AA-UHPC at 1, 3, 7, 14, 28, and 90 d of curing conditions showed that the ML models of LGBM, GBM, AdaBoost, BR, ETR, and RF, with accuracy percentages of 92.6%, 91.9%, 91.8%, 0.907%, 90.1%, and 90%, respectively, had the best estimations. The XGBoost, ERTR, RNNs, ESNs, RBFNs, HGBM, and CatBoost models had accuracies of 89.4% and 83.6%, respectively, while the ANNs and KNN had accuracies of 74.5% and 71.3%, respectively. The proposed Stacked ML models with active learning exhibited higher prediction accuracy values. Stacked ML-3, Stacked ML-1, Stacked ML-4, and Stacked ML-2 had prediction accuracies of 93.2%, 91.9%, 91.8%, and 90.5%, respectively, while active learning method can improve their accuracy to 98.9%, 95.9%, 94.5%, and 96.8%, respectively. Therefore, active learning can improve the accuracy between 2.6% till 4.1% and further enhance the Stacked ML models.
- The Stacked ML-3, LGBM, Stacked ML-1, Stacked ML-4, AdaBoost, and Stacked ML-2 models with lower score values were selected as the best prediction models. In contrast, the ESNs, CatBoost, RBFNs, RNNs, KNN, and ANNs models had the highest score values, indicating that their predictions were inaccurate.
- The validation results reveal that the Stacked ML models, including Stacked ML-3, Stacked ML-2, Stacked ML-1, and Stacked ML-4, achieved scores of 36, 72, 84, and 96, respectively, indicating their strong performance in predicting the compressive strength of AA-UHPC. When active learning was incorporated into these models, their performance improved significantly, with the updated models of AL-Stacked ML-3, AL-Stacked ML-2, AL-Stacked ML-1, and AL-Stacked ML-4, recording scores of 12, 24, 48, and 60, respectively. Consequently, these enhanced models were chosen as the most effective methods and were implemented in the GUI for practical use.
- A Stacked model of the ML algorithms was developed along with a GUI to provide a general model for predicting the compressive strength of AA-UHPC. Then experimental specimens have tested the capability of the GUI. The proposed GUI model can be conveniently used to reduce the experimental, numerical, and computational time and costs required to predict the outputs considered in this study.

Appendix

This appendix provides all specimen data points used for training and testing ML algorithms (Table 7).

Acknowledgements This work was done during outgoing mobility grant that was funded by the project "Gdańsk Tech Doctoral School closer to Europe" (project/contract number: BPI/STE/2023/1/00018/DEC/01; task internal number: 037162, acronym: "PG_go_West", hereafter: the Project), co-financed by the Polish National Agency for Academic Exchange (NAWA) under the Programme "STER—Internationalisation of Doctoral Schools".

Author contributions **Farzin Kazemi:** writing—original draft, software, methodology, funding acquisition, analysis, verification, conceptualization; **Torkan Shafighfard:** writing—original draft, data analysis, conceptualization, investigation; **Robert Jankowski:** supervision, writing—review and editing; **Doo-Yeol Yoo:** supervision, writing—review and editing.

Funding This study was supported by Polish National Agency for Academic Exchange.

Declarations

Conflict of interest The authors declare that they have no conflict of interest.

Ethical statement This research was done according to ethical standards.

Ethical approval This article does not contain any studies with human participants or animals performed by any of the authors.

References

1. Richard P, Cheyrezy M. Composition of reactive powder concretes. Cem Concr Res. 1995;25(7):1501–11.
2. Akeed MH, Qaidi S, Ahmed HU, Faraj RH, Mohammed AS, Emad W, Tayeh BA, Azevedo AR. Ultra-high-performance fiber-reinforced concrete. Part IV: durability properties, cost assessment, applications, and challenges. Case Stud Const Mater. 2022;17: e01271.
3. Piao R, Oh T, Kim GW, Choi HJ, Banthia N, Yoo DY. Enhanced microstructure and mechanical properties of cementless ultra-high-performance fiber-reinforced alkali-activated concrete with silicon dioxide nanoparticles. Const Build Mater. 2023;398:132514.
4. Larsen IL, Aasbakken IG, O'Born R, Vertes K, Thorstensen RT. Determining the environmental benefits of ultra high performance concrete as a bridge construction material. In IOP Confer Series Mater Sci Eng. 2017;245(5):052096.
5. Amran M, Roman F, Abdelgader HS, Murali G, Ozbakkaloglu T, Lee YH, Lee YY. Fiber-reinforced alkali-activated concrete: a review. J Build Eng. 2022;45:103638.
6. Zhang P, Wang K, Li Q, Wang J, Ling Y. Fabrication and engineering properties of concretes based on geopolymers/alkali-activated binders-a review. J Clean Prod. 2020;258: 120896.
7. Abdellatief M, Abadel AA, Federowicz K, Abd Elrahman M. Mechanical properties, high temperature resistance and microstructure of eco-friendly ultra-high performance geopolymer concrete: role of ceramic waste addition. Const Build Mater. 2023;401:132677.
8. Provis JL, Van Deventer JSJ (eds). Geopolymers: structures, processing, properties and industrial applications. Elsevier, 2009.
9. Heath A, Paine K, McManus M. Minimising the global warming potential of clay based geopolymers. J Clean Prod. 2014;78:75–83.
10. Zhang R, He H, Song Y, Zhi X, Fan F. Influence of mix proportioning parameters and curing regimes on the properties of ultra-high strength alkali-activated concrete. Constr Build Mater. 2023;393: 132139.
11. Sun B, Sun Y, Ye G, De Schutter G.A mix design methodology of blast furnace slag and fly ash-based alkali-activated concrete. Cement Concr Compos 2023;140:105076.
12. Hao Y, Yang G, Liang K. Development of fly ash and slag based high-strength alkali-activated foam concrete. Cement Concr Compos. 2022;128: 104447.
13. Lee SW, Kim GW, Oh T, You I, Wang X, Yoo DY. The microstructure and mechanical properties of cementless ultra-high-performance alkali activated concrete considering geometrical properties of steel fiber. Cement Concr Compos. 2023;142:105209.
14. Wetzel A, Middendorf B. Influence of silica fume on properties of fresh and hardened ultra-high performance concrete based on alkali-activated slag. Cement Concr Compos. 2019;100:53–9.
15. Yang Y, Huang Le, Lihua Xu, Min Yu, Ye H, Chi Y. Temperature-dependent compressive stress-strain behaviors of alkali-activated slag-based ultra-high strength concrete. Constr Build Mater. 2022;357: 129250.
16. Fan MX, Chen FX, Zhang XY, Wang RK, Yu R. Effect of Ca/Si ratio on the characteristics of alkali-activated ultra-high performance concrete (A-UHPC): from hydration kinetics to microscopic structure development. Constr Build Mater. 2023;394: 132158.
17. Kim GW, Oh T, Lee SK, Banthia N, Yoo DY. Development of Ca-rich slag-based ultra-high-performance fiber-reinforced geopolymer concrete (UHP-FRGC): Effect of sand-to-binder ratio. Constr Build Mater. 2023;370:130630.
18. Liang G, Yao W, Wei Y. A green ultra-high performance geopolymer concrete containing recycled fine aggregate: Mechanical properties, freeze-thaw resistance and microstructure. Sci Total Environ. 2023;895:165090.
19. Kim GW, Oh T, Lee SK, Lee SW, Banthia N, Yu E, Yoo DY. Hybrid reinforcement of steel–polyethylene fibers in cementless ultra-high performance alkali-activated concrete with various silica sand dosages. Constr Build Mater. 2023;394:132213.
20. Shen J, Li Y, Lin H, Li H, Lv J, Feng S, Ci J. Prediction of compressive strength of alkali-activated construction demolition waste geopolymers using ensemble machine learning. Constr Build Mater. 2022;360: 129600.
21. Bagherzadeh F, Shafighfard T, Khan RMA, Szczuko P, Mieloszyk M. Prediction of maximum tensile stress in plain-weave

composite laminates with interacting holes via stacked machine learning algorithms: a comparative study. Mech Syst Signal Process. 2023;195: 110315.
22. Shafighfard T, Kazemi F, Bagherzadeh F, Mieloszyk M, Yoo DY. Chained machine learning model for predicting load capacity and ductility of steel fiber–reinforced concrete beams. Comput Aided Civil Infrastr Eng. 2024. https://doi.org/10.1111/mice.13164.
23. Kazemi F, Shafighfard T, Yoo D-Y. Data-driven modeling of mechanical properties of fiber-reinforced concrete: a critical review. Arch Comput Methods Eng. 2024;31(4):2049–78.
24. Abdellatief M, Hassan YM, Elnabwy MT, Wong LS, Chin RJ, Mo KH. Investigation of machine learning models in predicting compressive strength for ultra-high-performance geopolymer concrete: a comparative study. Constr Build Mater. 2024;436:136884.
25. Abdellatief M, Abd Elrahman M, Abadel AA, Wasim M, Tahwia A. Ultra-high performance concrete versus ultra-high performance geopolymer concrete: mechanical performance, microstructure, and ecological assessment. J Build Eng. 2023;79:107835.
26. Kazemi F, Asgarkhani N, Jankowski R. Predicting seismic response of SMRFs founded on different soil types using machine learning techniques. Eng Struct. 2023;274: 114953.
27. Asgarkhani N, Kazemi F, Jankowski R. Active learning on ensemble machine-learning model to retrofit buildings under seismic mainshock-aftershock sequence. In: International Conference on Computational Science 2024; pp. 470–478.
28. Kazemi F, Asgarkhani N, Shafighfard T, Jankowski R, Yoo DY. Machine-learning methods for estimating performance of structural concrete members reinforced with fiber-reinforced polymers. Arch Comput Methods Eng 2024;1–33.
29. Kazemi F, Jankowski R. Machine learning-based prediction of seismic limit-state capacity of steel moment-resisting frames considering soil-structure interaction. Comput Str. 2023;274: 106886.
30. Sun Y, Cheng H, Zhang S, Mohan MK, Ye G, De Schutter G. Prediction & optimization of alkali-activated concrete based on the random forest machine learning algorithm. Constr Build Mater. 2023;385:131519.
31. Gomaa E, Han T, ElGawady M, Huang J, Kumar A. Machine learning to predict properties of fresh and hardened alkali-activated concrete. Cement Concr Compos. 2021;115: 103863.
32. ASTM C1856/C1856M-17. Standard Practice for Fabricating and Testing Specimens of Ultra-high Performance Concrete. ASTM International, West Conshohocken, PA 2017.
33. Cai R, Tian Z, Ye H. Durability characteristics and quantification of ultra-high strength alkali-activated concrete. Cement Concr Compos. 2022;134: 104743.
34. Huang Le, Liu J-C, Cai R, Ye H. Mechanical degradation of ultra-high strength alkali-activated concrete subjected to repeated loading and elevated temperatures. Cement Concr Compos. 2021;121: 104083.
35. Cai R, Ye H. Clinkerless ultra-high strength concrete based on alkali-activated slag at high temperatures. Cem Concr Res. 2021;145: 106465.
36. Liu J-C, Chen Z, Cai R, Ye H. Quantitative effects of mixture parameters on alkali-activated binder-based ultra-high strength concrete at ambient and elevated temperatures. J Adv Concr Technol. 2022;20(1):1–17.
37. Glanz D, Sameer H, Göbel D, Wetzel A, Middendorf B, Mostert C, Bringezu S. Comparative environmental footprint analysis of ultra-high-performance concrete using Portland cement and alkali-activated materials. Front Built Environ. 2023;9:1196246.
38. Wetzel A, Göbel D, Schleiting M, Wiemer N, Middendorf B. Bonding behaviour of steel fibres in UHPFRC based on alkali-activated slag. Materials. 2022;15(5):1930.
39. Shi K, Deng H, Hu J, Zhou J, Cai X, Liu Z. Effect of steel slag powder content and curing condition on the performance of alkali activated materials Based Ultra-High Performance Concrete (UHPC) Matrix. 2023.
40. Tahwia AM, Heniegal AM, Abdellatief M, Tayeh BA, Abd Elrahman M. Properties of ultra-high performance geopolymer concrete incorporating recycled waste glass. Case Stud Constr Mater. 2022;17: e01393.
41. Lao J-C, Ling-Yu Xu, Huang B-T, Dai J-G, Shah SP. Strain-hardening Ultra-High-Performance Geopolymer Concrete (UHPGC): matrix design and effect of steel fibers. Compos Commun. 2022;30: 101081.
42. Aisheh YI, Atrushi DS, Akeed MH, Qaidi S, Tayeh BA. Influence of steel fibers and microsilica on the mechanical properties of ultra-high-performance geopolymer concrete (UHP-GPC). Case Stud Constr Mater. 2022;17:e01245.
43. Xu S, Yuan P, Liu J, Pan Z, Zhongxian Liu YuSu, Li J, Chengqing Wu. Development and preliminary mix design of ultra-high-performance concrete based on geopolymer. Constr Build Mater. 2021;308: 125110.
44. Mousavinejad SH, Sammak M. Strength and chloride ion penetration resistance of ultra-high-performance fiber reinforced geopolymer concrete. Structures. 2021;32:1420–7.
45. Aisheh YI, Atrushi DS, Akeed MH, Qaidi S, Tayeh BA. Influence of polypropylene and steel fibers on the mechanical properties of ultra-high-performance fiber-reinforced geopolymer concrete. Case Stud Constr Mater. 2022;17: e01234.
46. Liu Y, Shi C, Zhang Z, Li N. An overview on the reuse of waste glasses in alkali-activated materials. Resour Conserv Recycl. 2019;144:297–309.
47. Ambily PS, Ravisankar K, Umarani C, Dattatreya JK, Iyer NR. Development of ultra-high-performance geopolymer concrete. Mag Concr Res. 2014;66(2):82–9.
48. Lao J-C, Ling-Yu Xu, Huang B-T, Zhu J-X, Khan M, Dai J-G. Utilization of sodium carbonate activator in strain-hardening ultra-high-performance geopolymer concrete (SH-UHPGC). Front Mater. 2023;10:1142237.
49. Guler S, Akbulut ZF. The single and hybrid use of steel and basalt fibers on high-temperature resistance of sustainable ultra-high performance geopolymer cement mortars. Str Concrete. 2023;24(2):2402–19.
50. Kathirvel P, Sreekumaran S. Sustainable development of ultra high performance concrete using geopolymer technology. J Build Eng. 2021;39: 102267.
51. Mousavinejad SH, Sammak M. An assessment of the effect of Na2SiO3/NaOH ratio, NaOH solution concentration, and aging on the fracture properties of ultra-high-performance geopolymer concrete: The application of the work of fracture and size effect methods. Structures. 2022;39:434–43.
52. Zhang Y, Chen J, Xia J. Compressive strength and chloride resistance of slag/metakaolin-based ultra-high-performance geopolymer concrete. Materials. 2022;16(1):181.
53. Aydın S, Baradan B. The effect of fiber properties on high performance alkali-activated slag/silica fume mortars. Compos B Eng. 2013;45(1):63–9.
54. Liu Y, Shi C, Zhang Z, Li N, Shi Da. Mechanical and fracture properties of ultra-high performance geopolymer concrete: effects of steel fiber and silica fume. Cement Concr Compos. 2020;112: 103665.
55. Asgarkhani N, Kazemi F, Jakubczyk-Gałczyńska A, Mohebi B, Jankowski R. Seismic response and performance prediction of steel buckling-restrained braced frames using machine-learning methods. Eng Appl Artif Intell. 2024;128: 107388.
56. Kazemi F, Asgarkhani N, Jankowski R. Machine learning-based seismic fragility and seismic vulnerability assessment of reinforced concrete structures. Soil Dyn Earthq Eng. 2023;166: 107761.

57. Asgarkhani N, Kazemi F, Jankowski R. Machine learning-based prediction of residual drift and seismic risk assessment of steel moment-resisting frames considering soil-structure interaction. Comput Str. 2023;289: 107181.
58. Shafighfard T, Bagherzadeh F, Rizi RA, Yoo DY. Data-driven compressive strength prediction of steel fiber reinforced concrete (SFRC) subjected to elevated temperatures using stacked machine learning algorithms. J Mater Res Technol. 2022;21:3777–94.
59. Kazemi F, Asgarkhani N, Jankowski R. Machine learning-based seismic response and performance assessment of reinforced concrete buildings. Arch Civil Mech Eng. 2023;23(2):94.
60. Bagherzadeh F, Shafighfard T. Ensemble Machine Learning approach for evaluating the material characterization of carbon nanotube-reinforced cementitious composites. Case Stud Constr Mater. 2022;17: e01537.
61. Shafighfard T, Kazemi F, Asgarkhani N, Yoo DY. Machine-learning methods for estimating compressive strength of high-performance alkali-activated concrete. Eng Appl Artific Intellig. 2024. https://doi.org/10.1016/j.engappai.2024.109053.
62. Kazemi Farzin, Asgarkhani Neda, Jankowski Robert. Optimization-based stacked machine-learning method for seismic probability and risk assessment of reinforced concrete shear walls. Expert Syst Appl. 2024;255:124897.
63. Liu Y, Zhang Z, Shi C, Zhu D, Li N, Deng Y. Development of ultra-high performance geopolymer concrete (UHPGC): influence of steel fiber on mechanical properties. Cement Concr Compos. 2020;112: 103670.
64. Standard ASTM. ASTM C109-standard test method for compressive strength of hydraulic cement mortars. ASTM International, West Conshohocken PA 2008.